The Lukoganskoe Au–Cu Skarn Deposit (Eastern Transbaikalia): Mineral Composition, Age, and Formation Conditions

Yu.O. Redin[a, ✉], A.A. Redina[a], I.R. Prokopiev[a,b], V.F. Dultsev[a,c], M.V. Kirillov[a], V.P. Mokrushnikov[a]

[a] V.S. Sobolev Institute of Geology and Mineralogy, Siberian Branch of the Russian Academy of Sciences,
pr. Akademika Koptyuga 3, Novosibirsk, 630090, Russia

[b] Novosibirsk State University, ul. Pirogova 1, Novosibirsk, 630090, Russia

[c] Kazan Federal University, ul. Kremlevskaya 4, Kazan, 420000, Russia

Abstract—The Lugokanskoe deposit is located in southeastern Transbaikalia and has been studied for a long time by many researchers. However, the type of its formation is still debatable. In this paper we study the mineral composition of ores by modern methods, recognize and describe the main gold mineral assemblages, and present detailed data on the chemical composition of native gold and sulfide minerals and their isotope composition. We have established that gold–pyrite–chalcopyrite–arsenopyrite and gold–bismuth parageneses localized in skarn deposits are the main productive assemblages. Study of the sulfur isotope composition of sulfide minerals has shown an endogenous source of sulfur of the ore minerals. The carbon and oxygen isotope compositions of carbonates of ore-bearing veins indicate the participation of a magmatic fluid. The established age of the gold mineralization and igneous rocks of the Shakhtama complex, together with direct geological observations, points to their spatial, temporal, and genetic relationships. According to their petrochemical and geochemical characteristics, the igneous rocks of the Shakhtama complex are *I*-type ilmenite (reduced) granitoids. Study of fluid inclusions by heating and cooling and Raman spectroscopy has shown that the mineral formation was accompanied by a gradual decrease in the content of salts in the ore-forming fluids and by a decrease in their homogenization temperatures. Optical observations demonstrate that the fluid was heterogeneous at the early stages of the mineral formation. The evolution of the ore system was accompanied by a change in the gas phase composition of fluid inclusions from predominantly nitrogen–carbon dioxide to essentially aqueous, with carbon dioxide impurity $(H_2O + CO_2 \pm N_2 \rightarrow H_2O \pm CO_2)$. The research data testify to the magmatic nature of fluids and the participation of meteoric waters at the late stages of the ore-forming process. The data obtained have led to the conclusion that the Lugokanskoe gold deposit is related to reduced intrusions formed at a shallow depth.

Keywords: Au–Cu skarn deposits, reduced granitoids, eastern Transbaikalia

INTRODUCTION

The problem of the sources of ore substance and the relationship of endogenous deposits with igneous rocks has received much attention for a long time (Sillitoe, 1991; Hedenquist and Lowenstern, 1994; Thompson et al., 1999; Nie et al., 2004; Bierlein and Mcknight, 2005; Mel'nikov et al., 2009; Arzamastsev et al., 2010; Pavlova et al., 2010; Garmaev et al., 2013; Goldfarb et al., 2014). Mesozoic igneous rocks occupy a special place in the geology of Transbaikalia. The most commercially important specifics of Mesozoic magmatism is that it gave rise to endogenous deposits of nonferrous, rare, and noble metals (Spiridonov et al., 2006). Intrusive rocks of the Shakhtama complex are widespread within the Argun' (Shakhtama, Lugokan, Bystraya,

and other massifs) and Aga (Budulan, Tsasuchei, Goshunov, Imalka, and other massifs) zones of Transbaikalia. In southeastern Transbaikalia, there are the largest gold and complex deposits spatially associated with the Shakhtama complex: Lugokanskoe, Kultuminskoe, Bystrinskoe, Bugdainskoe, etc. (Fig. 1).

All the above deposits have a number of similar features, first of all, localization at the intersection of deep faults, spatial association with the igneous rocks of the Shakhtama complex, close ages, etc. One of them is the Lugokanskoe deposit, where porphyry Au–Cu–Mo (Sazonov, 1978; Sizykh and Sizykh, 2001; Bessonov, 2009) and Au–Cu skarn (Kormilitsyn and Ivanova, 1968; Skurskii, 1996) types of mineralization are recognized. At present, many researchers distinguish a special class of gold deposits, namely, intrusion-related gold systems (IRGS), which are among the major sources of gold (Pirajno, 2009). They are subdivided into deposits related to oxidized intrusions (porphyry copper de-

✉Corresponding author.
   E-mail address: redin@igm.nsc.ru (Yu.O. Redin)
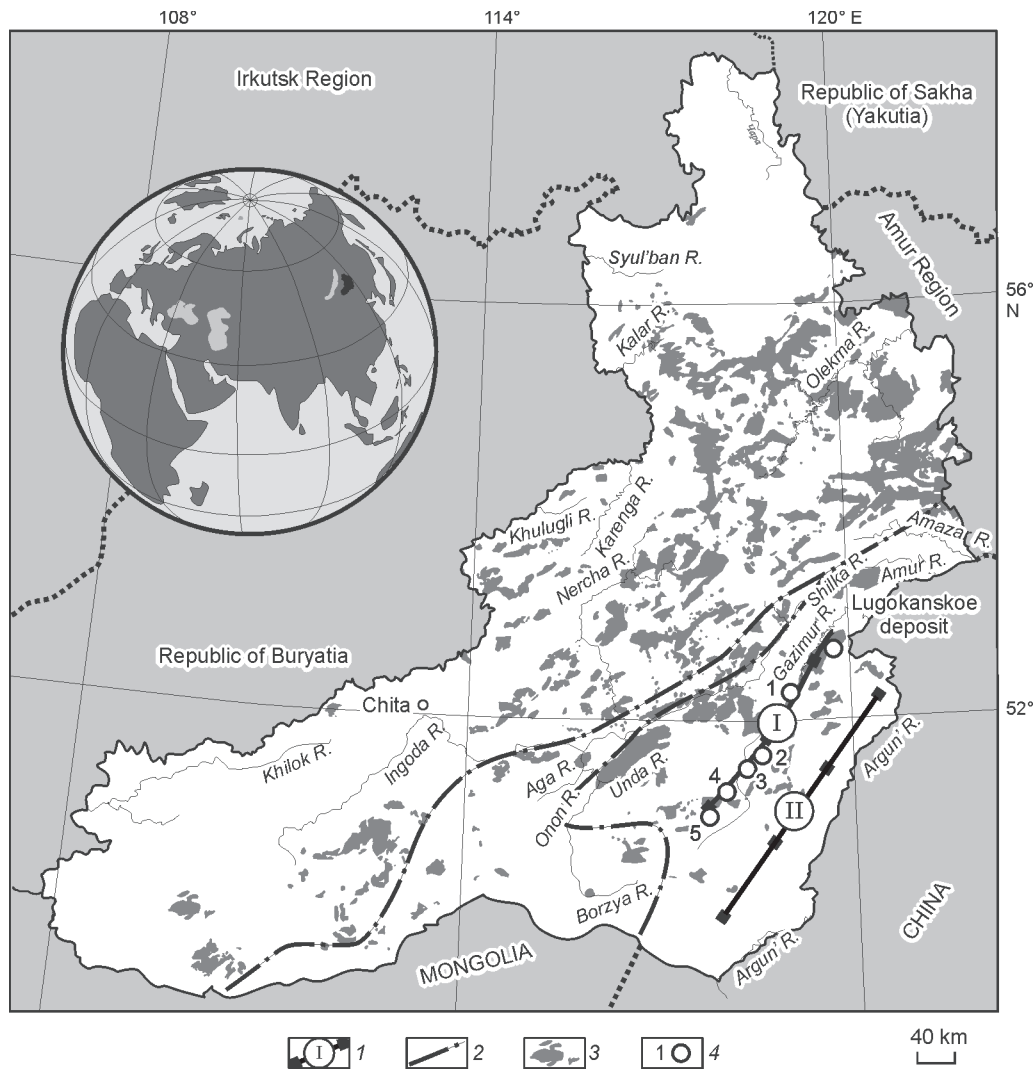
Fig. 1. Regional position of gold and complex deposits spatially associated with the Shakhtama intrusive complex, after Redin and Kozlova (2014), supplemented. *1*, regional fault zones (I, Gazimur, II, Urulyungui); *2*, Mongolo–Okhotsk suture; *3*, Late Jurassic igneous associations; *4*, deposits: 1, Kultuminskoe; 2, Novoshirokinskoe, Lugiinskoe, etc.; 3, Bystrinskoe; 4, Shakhtaminskoe; 5, Bugdainskoe.

posits) and to reduced intrusions (RIRGD). A model for IRGS was elaborated mostly by the example of the gold objects of Central Alaska and Yukon, where they are part of the Tintina Gold Province including well-known deposits, such as Fort Knox (Bakke, 1995), Dublin Gulch (Maloof et al., 2001), Clear Creek (Marsh et al., 2003), and Scheelite Dome (Mair, 2004). In this paper we consider the genesis of the Lugokanskoe deposit, based on geological, petrographic, petrochemical, mineralogical, geochemical, isotope-geochronological, and physicochemical data.

MATERIALS AND METHODS

We studied ores sampled from trenches and boreholes of the deposit. The compositions, structures, and textures of minerals and relationships among them were examined under an optical microscope, in reflected and transmitted light.

Monomineral fractions of arsenopyrite, pyrite, and other sulfides were taken (under a binocular) from crushed rocks and sulfide concentrates obtained on the dissolution of the samples in hydrofluoric acid. The chemical composition of sulfides and native gold was determined in polished grains by electron probe microanalysis (JEOL JXA-8100 electron microprobe) and by scanning electron microscopy (SEM) (JSM-6510 scanning electron microscope equipped with an OXFORD energy-dispersive spectrometer). The isotopic compositions of sulfur in sulfide minerals and of oxygen and carbon in carbonates were measured at the Analytical Center for Multi-Elemental and Isotope Research, SB RAS, Novosibirsk. The error of determination of $\delta^{34}S_{CDT}$ (1σ) was 0.1‰. Carbonates were decomposed with orthophosphoric acid at 60–70 ºC for 2–4 h, using the Gas Bench option. All measurements were made on a Finnigan MAT 253 mass spectrometer in the constant helium flow mode. The $\delta^{13}C_{PDB}$

and $\delta^{18}O_{SMOW}$ values were determined with an error of ±0.05 and ±0.1‰ (1σ), respectively.

Fluid inclusions were studied in transparent polished plates by heating and cooling and Raman spectroscopy. Heating/cooling studies were performed on a Linkam THMSG-600 thermal microstage. The composition of the gas phase of fluid inclusions was studied by Raman spectroscopy (Ramanor U-1000 spectrometer and Horiba DU420E-OE-323 detector (Jobin Yvon), Millennia Pro laser (Spectra-Physics); alpha300R confocal Raman microscope (WITec)).

The $^{40}Ar/^{39}Ar$ isotope-geochronological dating with stepwise heating was used to establish the absolute age of igneous rocks and mineralization.

The content of major elements in igneous rocks was determined by X-ray fluorescence analysis, and the contents of trace and rare-earth elements, by ICP MS (ELEMENT (Finnigan MAT) high-resolution mass spectrometer with a U-5000AT+ ultrasonic nebulizer). Analysis of rock-forming components (SiO_2, TiO_2, Al_2O_3, Fe_2O_3, FeO, MnO, MgO, CaO, P_2O_5, Na_2O, K_2O, H_2O, and LOI) in the igneous rocks was also made by the solution chemistry method in the chemical group of the Geodynamics and Geochronology Common Use Center of the Institute of the Earth's Crust, Irkutsk.

GEOLOGIC STRUCTURE
OF THE LUGOKANSKOE DEPOSIT

General outlines of the geotectonic position. The Lugokanskoe deposit is located in the central part of the Lugokan ore cluster (Fig. 2), in the Aga–Borzya structural-formation zone of the Mongol–Okhotsk orogenic belt. Two major stages of the belt formation are clearly recognized: Paleozoic and Mesozoic. Its main structural components (fragments of early Paleozoic oceanic blocks, middle Paleozoic subduction island-arc volcanic belts, late Paleozoic continent-marginal volcanic belts, and areas of orogenic granitic magmatism) formed at the Paleozoic stage (Goryachev et al., 2014).

The closure of the Mongol–Okhotsk Ocean and the collision of the continent-marginal complexes of the Siberian and North Mongolia–Chinese continents took place at the Early–Middle Jurassic boundary. The processes related to the collision (thrusting, folding, metamorphism, and magmatism) occurred throughout the Middle Jurassic and most of the Late Jurassic. The transition to extension processes, accompanied by the formation of metamorphic cores and sedimentary troughs, dates back to the late Late Jurassic–Early Cretaceous. The Early Cretaceous intracontinental rifting might have been caused by the collapse ("spreading") of the collisional uplift after the termination of compression and by the mantle convection related to the active hot spot overlapped by the continental lithosphere (Zorin et al., 2001; Spiridonov et al., 2006).

The ore cluster comprises three deposits (Lugokanskoe, Serebryanoe, and Solonechenskoe). By metallogeny, it is part of the Budyumkan–Kultuma ore district (Au, Cu, Pb, Zn, and Sn) located between the Gazimur, Budyumkan, and Uryumkan Rivers. The Gazimur–Uryumkan interfluve is a mining area with widespread gold–polymetallic and rare-metal mineralization.

The host rocks. The geologic section of the Lugokanskoe deposit includes a Paleozoic shale–carbonate unit intruded by granodiorite-porphyry bodies of the Shakhtama complex ($\gamma\delta\pi J_{2-3}s$) (Fig. 3), which are overlain by a terrigenous-volcanic member of the Glushkovo Formation in the northwestern part of the area (J_3gl_1).

Deposits of the lower Cambrian Bystraya Formation ($\mathcal{E}_1bs$) are the oldest. They occupy most of the deposit area and are predominantly carbonate rocks (limestones, dolomites, and their transitional varieties) with intercalates and lenses of variably metamorphosed terrigenous rocks (carbonaceous, mica, biotite–amphibole, and other schists).

Terrigenous rocks of the Il'dikan Formation ($D_{1-2}il$) are less spread; they occur in the southwest of the Lugokanskoe deposit area. These are quartz–feldspar–mica schists. Poor pyritization is observed almost everywhere. The rocks are partly carbonized and graphitized.

Rocks of the Glushkovo Formation (J_3gl_1) are found only in the northern part of the deposit. These are basaltic trachyandesites, basaltic andesites, dolerites, and their tuffs; seldom, pebble conglomerates and sandstones are present.

There are also explosive breccias, the youngest rocks of the deposit. They consist of fragments of quartz, devitrified glass, and single phenocrysts of mica, apatite, and chalcedony-like and colloform quartz saturated with ore dust. The breccia cement contains a volcanic tuff material.

Structures and textures. The tectonic structure of the deposit is determined by a combination of widespread folds and faults of different ranks and ages. The main and most ancient structure here is the Lugokan asymmetric anticline of NW strike, complicated by a series of higher-rank brachiform and linear folds. The anticline asymmetry is expressed as a steep (up to subvertical) dip of its southwestern flank and a gentle dip of its northeastern flank.

The location of the deposit at the intersection of differently oriented (northeastern Budyumkan and northwestern Urov–Dzhalir) regional faults led to intense brittle deformations here. The latter are expressed as numerous fracture, crush, and rock brecciation zones. All faults form a single tectonic zone of NW direction with predominant SW and subordinate NE dips. The zone is about 9 km in total length and up to 2 km in width. The main zone structures are confined to the contacts (northeastern and southwestern) of the major intrusion fragment.

Magmatism. Intrusive rocks of the Lugokan massif belong to the second phase of the Middle–Late Jurassic Shakhtama complex. Granodiorite-porphyry and granite-porphyry with fine phenocrysts are spread in the northwestern part of the massif. In the central part they are changed by granodiorite-porphyry with coarse porphyry phenocrysts, which grade into porphyritic granodiorites in the east. This
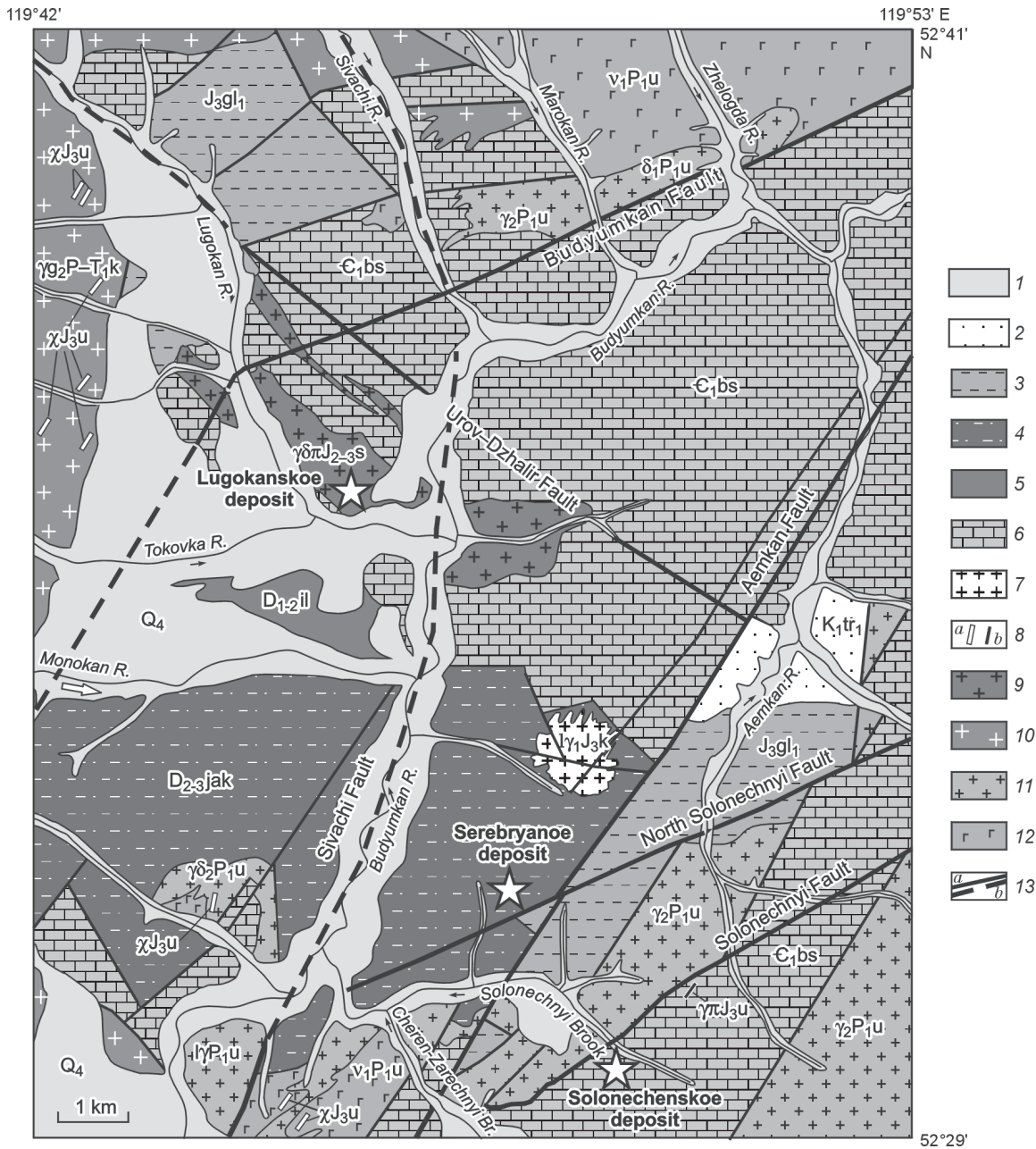
Fig. 2. Schematic geological map of the Lugokan ore cluster, after Redin and Kozlova (2014), supplemented. *1*, Quaternary deposits (Q_4); *2*, Turga Formation (K_1tr_1), conglomerates; *3*, Glushkovo Formation (J_3gl_1), conglomerates, sandsontes, siltstones, and basalt-trachyandesitic, basalt-andesitic, andesitic, and basaltic lavas; *4*, Yakovlevka Formation ($D_{2-3}jak$), sandstones, siltstones, and limestones; *5*, Il'dikan Formation ($D_{1-2}il$), mica and quartz–mica schists; *6*, Bystraya Formation ($Є_1bs$), limestones and dolomites; *7*, Kukul'bei complex ($l\gamma_1J_3k$), leucogranites; *8*, Unda–Daya complex (J_3u): *a*, lamprophyre and hybrid porphyry dikes, *b*, granite-porphyry dikes; *9*, Shakhtama complex ($\gamma\delta\pi J_{2-3}s$), granodiorite-porphyry; *10*, Kutomara complex ($\gamma g_2P–T_1k$), gneiss-granites; *11*, *12*, Unda complex (P_1u): *11*, leucocratic granites ($l\gamma_3$), granites (γ_2), and granodiorites ($\gamma\delta_2$) and diorites (δ_1), *12*, gabbro (ν_1); *13*, faults: *a*, proved, *b*, predicted.

facies horizontal zoning indicates a deeper erosional truncation of the eastern part of the intrusion as compared with the central and northwestern parts. The absolute K–Ar age of granodiorite-porphyry is 178–157 Ma (Sazonov, 1978). The Ar^{39}/Ar^{40} plateau age of biotite from granodiorite-porphyry of the Lugokan massif (Table 1, No. 7) is 154.7 ± 1.2 Ma (Fig. 4).

The average surficial size of the intrusion is 8.6 × 1.1 km. The intrusion is confined to the intersection of the northeastern Budyumkan and northwestern Urov–Dzhalir regional faults, forming mainly the southwestern and, less, northeastern flanks and the end of the Lugokan anticline. As shown by mining and drilling performed by OOO Vostokgeologiya, the Lugokan intrusion rocks within the studied part of
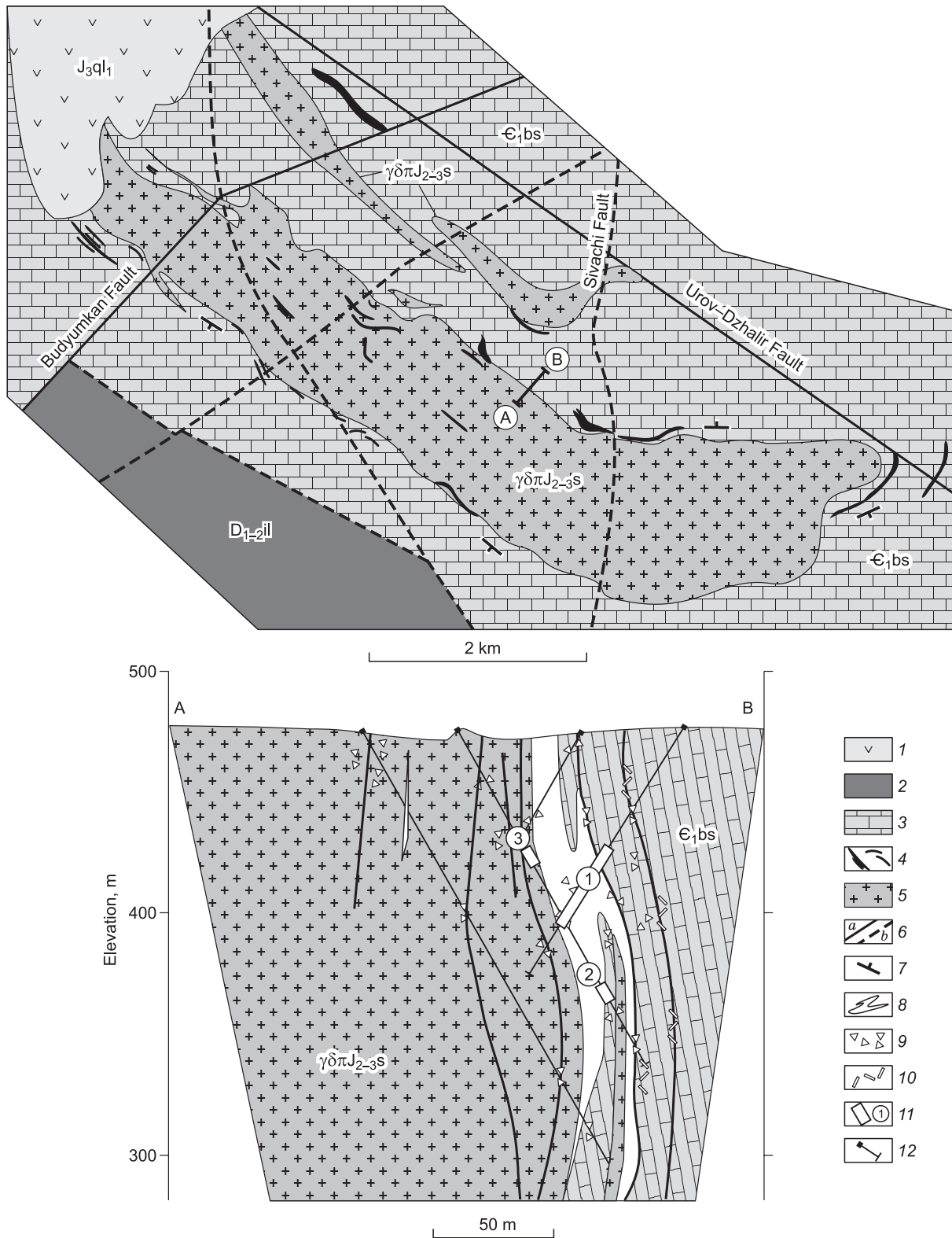
Fig. 3. Geological scheme and section of the Lugokanskoe deposit, compiled after the OOO Vostokgeologiya data. *1*, Glushkovo Formation (J_3gl_1), basaltic trachyandesites, basaltic andesites, and dolerites; *2*, Il'dikan Formation ($D_{1-2}il$), mica and quartz–mica schists; *3*, Bystraya Formation (C_1bs), limestones and dolomites; *4*, dike series; *5*, Shakhtama complex ($\gamma\delta\pi J_{2-3}s$), granodiorite porphyry; *6*, faults: *a*, proved, *b*, predicted; *7*, inclined bedding; *8*, skarns; *9*, brecciation and shearing zones; *10*, mylonitization zones; *11*, ore intervals (our data): 1, 2, Au–Bi mineralization, 3, pyrite–pyrrhotite–chalcopyrite mineralization; *12*, boreholes.

Table 1. Chemical composition of the igneous rocks of the Shakhtama complex (wt.%), Budyumkan–Kultuma ore district

No.	SiO_2	TiO_2	Al_2O_3	FeO	Fe_2O_3	MnO	MgO	CaO	Na_2O	K_2O	P_2O_5	LOI	Total
	Granodiorite-porphyry, Lugokan massif, after Sazonov (1978)												
1	66.54	0.71	15.12	3.01	0.53	0.05	2.30	3.30	3.80	3.70	0.09	1.00	100.15
2	66.56	0.81	14.82	1.44	0.69	0.03	1.82	4.97	4.00	3.40	0.09	1.40	100.03
3	66.50	0.76	15.12	1.72	0.49	0.03	1.82	4.85	3.65	3.40	0.09	1.30	99.73
4	65.95	0.65	15.02	2.80	0.85	0.05	1.90	3.42	3.70	3.60	0.11	1.45	99.50
	Granodiorite-porphyry, Lugokan massif, our data (solution chemistry method)												
5	64.34	0.48	14.42	2.69	0.53	0.04	2.37	4.73	3.82	3.03	0.14	2.68	99.27
6	64.23	0.50	14.90	2.89	0.38	0.04	2.34	4.61	3.82	3.04	0.14	2.64	99.53
7	65.76	0.42	14.89	1.38	0.56	0.02	2.05	4.39	3.67	3.61	0.13	1.21	98.09
8	66.72	0.46	15.61	1.75	0.66	0.02	2.65	3.21	3.91	3.63	0.13	1.21	99.96
9	66.65	0.48	15.61	1.74	0.66	0.03	2.69	3.23	3.85	3.65	0.13	1.22	99.94
	Monzonite-porphyry (dike series, Serebryanoe deposit), after Redin et al. (2015) (X-ray fluorescence, Fe_2O_{3tot})												
10	56.79	1.06	15.65	N.d.	8.91	0.06	4.95	4.04	3.69	3.24	0.30	0.98	99.67
11	57.05	0.90	15.12	N.d.	8.11	0.06	4.38	4.87	3.53	3.48	0.26	1.11	98.87
12	58.41	0.89	15.90	N.d.	7.09	0.03	4.55	5.61	2.30	4.18	0.18	2.17	101.31
13	61.99	0.91	15.29	N.d.	5.24	0.04	3.96	4.44	4.10	3.44	0.26	0.60	100.27
	Dioritic porphyrites (dike series, Lugokanskoe deposit), after Sazonov (1978)												
14	60.25	0.85	14.28	4.3	1.35	0.09	4.92	5.51	3.70	2.40	0.14	1.80	99.59
	Granodiorite-porphyry, Kultuma massif, our data (solution chemistry method)												
15	63.51	0.52	13.94	3.12	0.63	0.05	3.04	3.6	3.48	3.64	0.12	3.30	98.95

Note. N.d., not determined.

the deposit (to a depth of 300–350 m) form not a stock or a dike-like body, as previously believed, but a typical sill. In the near-contact zone of the massif, the host rocks are marbleized and skarnified, with the thickness of endo- and exoskarns varying from few centimeters to tens of meters and their length reaching few hundred meters. In places, sheared granodiorite-porphyry has numerous tourmaline and quartz–tourmaline veins. Dikes are formed by granodiorite-porphyry, granite-porphyry, and diorite porphyrites. Some researchers assign the dikes to the final phase of the Shakhtama complex (Sidorenko, 1961), whereas others consider them an individual porphyry complex (Sotnikov et al., 1977; Ber-
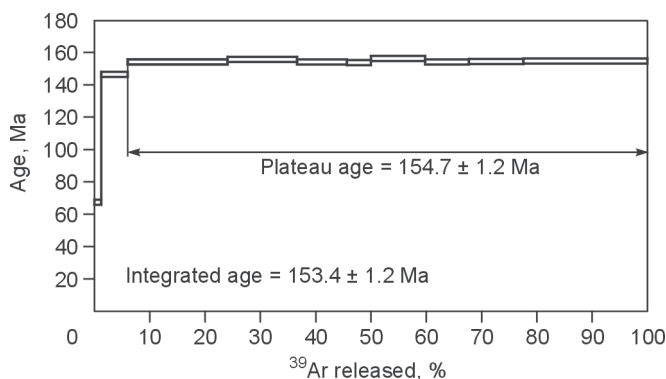
Fig. 4. The age of biotite from granodiorite-porphyry of the Lugokan massif.

zin et al., 2013). The Shakhtama complex bears commercial polymetallic, gold–polymetallic, gold, and rare-metal mineralization (Timofeevskii, 1972; Tauson, 1982; Tauson et al., 1987; Zorina, 1993; Koval', 1998; Prokof'ev et al., 2000; Spiridonov et al., 2006; Abramov, 2012).

Structure and morphology of orebodies. Mineralization is confined mainly to skarns, less, to carbonate rocks (undergone intense tectonic transformation), and, seldom, to granodiorite-porphyry. Orebodies are blanket, lenticular, and vein-like. Most orebodies occur subconformably with the intrusion contacts. In places, the orebody structure is clearly controlled by the skarn morphology. Skarns are most often observed in the near-contact zone of the massif, where monotonous carbonate strata are predominant. They are confined to the zones of the massif contact bends, where they are usually of the maximum thickness. These are zones with the most intense tectonic processes. The borders of the deposit orebodies are unclear and are established only by sampling. The rich and poor zones of the orebodies are spatially confined to areas of intense and weak brittle deformations, respectively. Several main types of ores are recognized according to their mineral composition: magnetite, scheelite–molybdenite, and gold–sulfide. Often, complex ores formed through telescoping are observed. Gold–sulfide ores are of commercial value. Magnetite ores occur only in skarns. Gold–sulfide ores concentrate mainly in skarns in the near-contact zone of the massif and are superposed on

them. They are also found in crush and brecciation zones in carbonate rocks. Molybdenite–scheelite ores have no commercial value and are of limited occurrence (scarce quartz veins in granodiorite-porphyry).

PETROCHEMISTRY AND GEOCHEMISTRY OF IGNEOUS ROCKS OF THE SHAKHTAMA COMPLEX

The Shakhtama intrusive complex was recognized by Yu.A. Bilibin and was long studied by many geologists. It includes stocks, laccoliths, and dike-like bodies of acid and intermediate composition. These are usually fractured or semiconcordant bodies. Their location is controlled by the sites of intersection of fault zones of different strikes. The complex comprises several intrusion phases. The first phase is monzodiorites, quartz monzonites, gabbro, and granosyenites. The second phase is predominant biotite–hornblende, often porphyritic, granodiorites and quartz syenites and subordinate granites, quartz monzonites, and quartz diorites. The third phase is small stock- and dike-like bodies of aplite-like granites, quartz syenites, and granosyenites. The final dike series is characterized by a wide spread of quartz syenite-porphyry, granodiorite-porphyry, granite-porphyry, monzonite-porphyry, and dioritic porphyrites (Spiridnov et al., 2006).

The Lugokan massif is composed predominantly of granodiorite-porphyry and, less, granite-porphyry. The main rock-forming minerals are plagioclase, quartz, K–Na-feldspar, biotite, and amphibole. The accessory minerals are apatite and zircon; often, rutile, anatase, orthite, and ilmenite and, seldom, magnetite are present.

There are small bodies and dikes within the Lugokan massif and the host rocks (Lugokanskoe deposit) and at a distance from it (Serebryanoe deposit). The final dike series (at the Serebryanoe deposit) is rocks varying in composition from monzonite-porphyry to granite-porphyry. Monzonite-porphyry and dioritic porphyrites are predominant; they have both subconformable and cutting contacts with the host rocks. Most of the bodies have a zonal structure: Their margins have a more basic composition and are formed by dioritic porphyrites, whereas the central part is made up of granodiorite-porphyry and plagiogranite-porphyry (Redin and Kozlova, 2014). The rocks are composed of plagioclase, K–Na-feldspar, quartz, biotite, and amphibole in different proportions. Phenocrysts amount to 10–50 vol.%. The accessory minerals are apatite, sphene, zircon, ilmenite, and, more seldom, magnetite. The Ar–Ar age of monzonite-porphyry is 154.6 ± 1.5 Ma (Redin and Kozlova, 2014).

Rock-forming components. The contents of rock-forming components are given in Table 1. The content of SiO_2 varies from 64.2 to 66.7 wt.% in rocks of the Lugokan massif and from 56.8 to 62.0 wt.% in rocks of the dike series. The igneous rocks of the massif and the dike series have, in general, a high total content of alkalies: $K_2O + Na_2O = 6.8$–
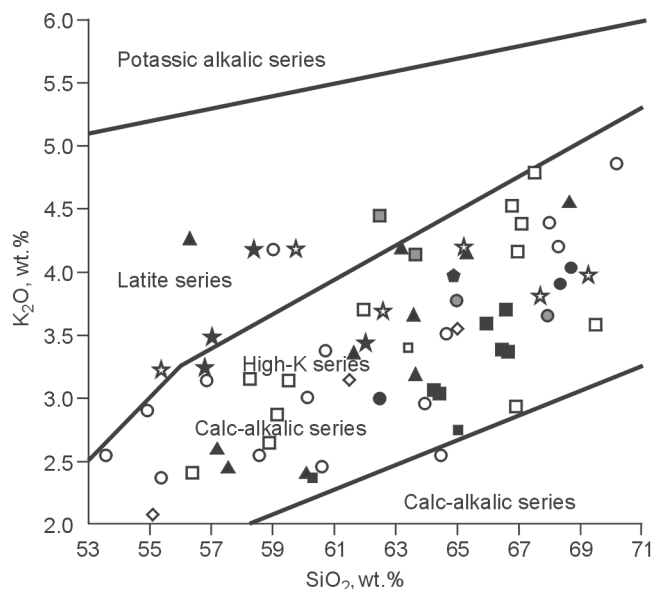
Fig. 5. K_2O–SiO_2 correlation in igneous rocks of the Shakhtama complex. *1*, Lugokan massif, after Sazonov (1978) and our data; *2*, dike series (Lugokan ore cluster (Redin et al., 2015)); *3*, Shakhtama massif (Pavlova and Tikhomirov, 1964); *4*, dike series (Shakhtama massif); *5*, Lugiya massif (Kormilitsyn and Ivanova, 1968); *6*, Bystraya massif (Spiridonov et al., 2006); *7*, Shiveya massif (Pavlova and Tikhomirov, 1964); *8*, Arkiya massif (Pavlova and Tikhomirov, 1964); *9*, Listvyanka massif (Pavlova and Tikhomirov, 1964); *10*, Kultuma massif; *11*, granitoid massifs of the Shakhtama complex of the Aga zone (Kozlov, 2011). Fields of rock series are given after Ewart and Taylor (1969), Peccerillo and Taylor (1976), Grill (1981), and Rickwood (1989).

7.5 and 6.1–7.5 wt.% ($K_2O = 3.0$–3.7 and 2.4–4.2 wt.%), respectively. In the K_2O–SiO_2 composition diagram, rocks of the Shakhtama complex lie mostly in the field of high-K calc-alkalic series (Fig. 5).

The studied igneous rocks are metaluminous: ASI ($Al_2O_3/(CaO - 1.67P_2O_5 + Na_2O + K_2O)$) = 0.77–0.97 for the Lugokan massif and 0.77–0.94 for the dike series.

To separate the igneous rocks of the Shakhtama complex into a magnetite and an ilmenite series, we used the diagram proposed by Ishihara (1977). As seen in Fig. 6, most of the figurative points of the Shakhtama complex rocks fall in the field of the ilmenite (reduced) series. In the Lugokan massif, the Fe_2O_3/FeO ratio is 0.13–0.48 in granodiorite-porphyry and 0.3 in dioritic porphyrites. The maximum Fe_2O_3/FeO values are typical of monzonites (2.1) and monzodiorites (1.2) of the Bystraya massif and monzonites (1.3) of the Shakhtama massif. High Fe_2O_3/FeO values are specific to granite-porphyry (0.9) of the Arkiya massif, granodiorites (0.9) of the Arkiya massif, and granodiorites (0.9) of the Shakhtama massif.

Trace elements. The dike series rocks have the following contents of elements (ppm): compatible elements— Ni = 48–96, Cr = 92–493, and V = 115–142; large-ion lithophile elements (LILE)—Rb = 94–173, Ba = 369–564, and Sr = 298–626; and high-strength field elements (HFSE)—
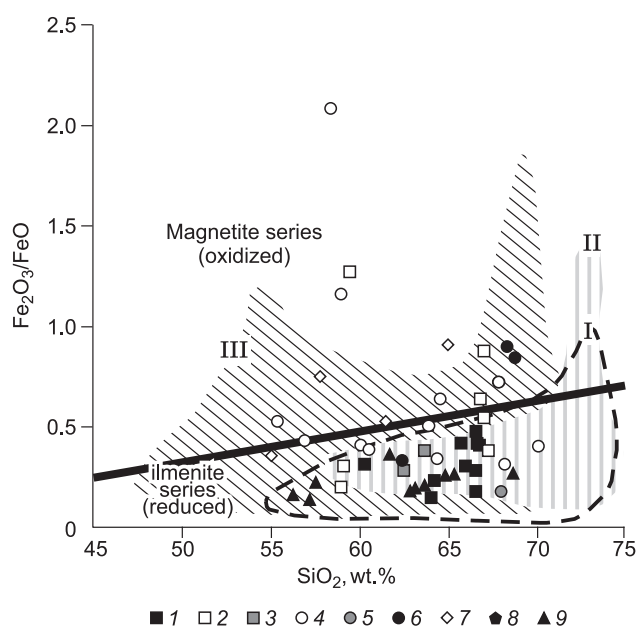
Fig. 6. Composition diagram (Ishihara, 1977) separating the magnetite and ilmenite series. Fields of igneous rocks (Hart et al., 2004): I, intrusions of the Yukon–Tanana Upland (Pogo Deposit); II, Fairbanks plutonic complex (Fort Knox Mine); III, Tombstone belt (Scheelite Dome deposit, Dublin Gulch, Clear Creek). *1*, Lugokan massif, after Sazonov (1978) and our data; *2*, Shakhtama massif (Pavlova and Tikhomirov, 1964); *3*, Lugiya massif (Kormilitsyn and Ivanova, 1968); *4*, Bystraya massif (Spiridonov et al., 2006); *5*, Shiveya massif (Pavlova and Tikhomirov, 1964); *6*, Arkiya massif (Pavlova and Tikhomirov, 1964); *7*, Listvyanka massif (Pavlova and Tikhomirov, 1964); *8*, Kultuma massif; *9*, granitoid massifs of the Shakhtama complex of the Aga zone (Kozlov, 2011).

Zr = 93–132 and Nb = 9.9–14.6. The igneous rocks have, in general, high contents of LREE, lower contents of MREE, and low contents of HREE. The contents of REE in monzonite-porphyry are as follows (ppm): La = 11–43, Sm = 2.1–9.4, Yb = 1.07–2.58, and Y = 15.06–29.47. The REE patterns show a negative slope, steep in the MREE region and gentle in the LREE and HREE regions, and a low negative Eu anomaly. The trace-element patterns of monzonite-porphyry show positive Rb, Th, and U anomalies and negative Nb and Ta anomalies (Redin et al., 2015).

Our results are consistent with the data on the Shakhtama deposit obtained by Berzina et al. (2013) (close ages and similar petrochemical and trace-element compositions of rocks), who first recognized the Shakhtama intrusive complex. The authors report that the Shakhtama complex formed at the end of collision, whereas the dike series (porphyry complex) appeared in the postcollisional (rifting) setting.

Another crucial specific feature of the Shakhtama complex is its initial enrichment in granitophile and trace elements (B, F, Li, Rb, Cs, Be, Sn, W, Mo, Nb, Ta, Th, and U) (Kozlov, 2011). The Clarke contents of rare metals in the Shakhtama complex indicate their magmatic origin not related to any superposed (e.g., hydrothermal) processes. Since the rare-metal signatures are observed in massifs of

different compositions, this means that the initial magmatic melts (independently of their subsequent crystallization differentiation and the formation of their petrochemically different derivates) were already enriched in granitophile trace elements (Kozlov, 2011).

MINERAL COMPOSITION AND FORMATION SEQUENCE OF ORES

One of the first research works on the Lugokanskoe deposit was published in the late 1970s (Sazonov, 1978). Earlier it was believed that the deposit ores are composed of a limited number of minerals: pyrite, arsenopyrite, chalcopyrite, bornite, sphalerite, galena, and antimonite. At present, more than 40 ore minerals have been found in the ores by the application of modern research methods. Chalcopyrite, pyrite, and arsenopyrite are major ore-forming minerals; pyrrhotite and magnetite are secondary minerals; bismuthine, sphalerite, galena, fahlores, and bornite are less spread; molybdenite, scheelite, tsumoite, cosalite, ingodite, tetradymite, emplectite, wittichenite, giessenite, kobellite, pecoite, friedrichite(?), schirmerite(?), native bismuth, hessite, aschamalmite(?), nuffieldite(?), native gold, etc. are rare. Sulfide ores are superposed on the host rocks (skarns). There are several varieties of skarns in the deposit: olivine, pyroxene–garnet, garnet, garnet–phlogopite, phlogopite–garnet, and phlogopite. They form both homogeneous and zoned bodies; the latter are composed of garnet skarns in the central part and garnet–phlogopite and phlogopite–garnet skarns on the margin. Olivine skarns are revealed in the northeast of the deposit and are of limited occurrence. The deposit ores have phenocryst, veinlet–phenocryst, nest–phenocryst, and, locally, massive, fractured, brecciform, and spotted textures and fine-, thin-, and coarse-grained structures. Major valuable components of the ores are copper, gold, and silver. The data presented below significantly supplement the earlier published information (Redin et al., 2014, 2015) about the composition of minerals and their relations and assemblages in the ores.

Typomorphic features of the ore minerals. Phlogopite is among the most abundant skarn minerals. Its content in phlogopite skarns reaches 90%, whereas in garnet–phlogopite and phlogopite–garnet skarns it amounts to 30–60%. Phlogopite contains (wt.%, SEM data) K_2O = 7.9–9.6, MgO = 22.8–24.0, TiO_2 = 0.7–0.9), and F = 2.0–2.6.

Garnet occurs as irregular-shaped and round grains and intergrown crystals measuring 0.*n* to 3 mm. By chemical composition, garnets are mostly andradite with impurities of TiO_2, Al_2O_3, and MnO. Garnets often have a zonal structure (Fig. 7*c*); there are both normal (direct) zoning and oscillatory zoning marking fluctuations of the same components as the direct one. The normal zoning is expressed as an increase in the content of the andradite end-member and a decrease in the content of the grossular end-member from core to edge of the garnet crystals and marks the natural course of
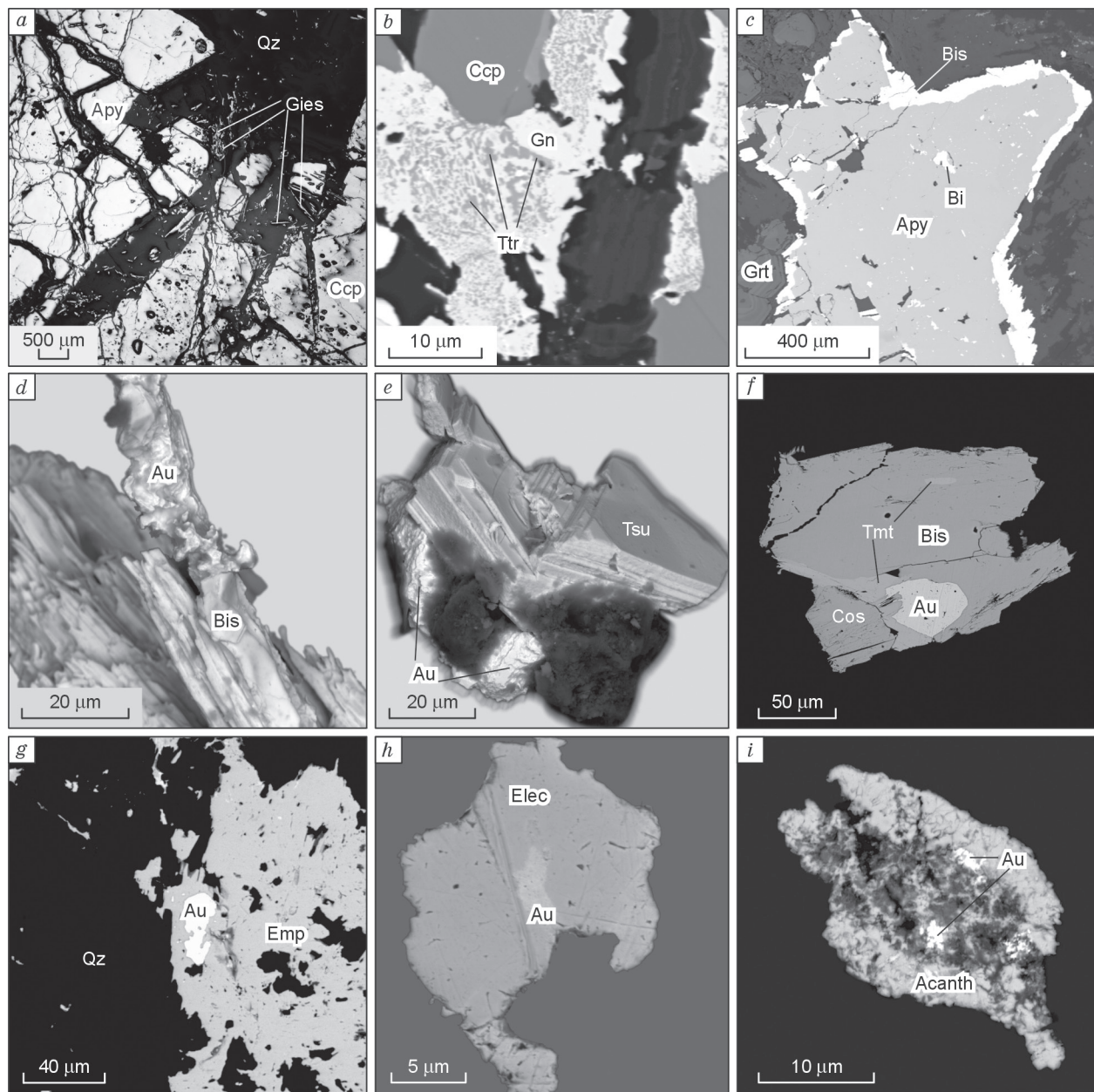
Fig. 7. Mineral assemblages of the Lugokanskoe deposit. *a*, Typical relations of arsenopyrite and chalcopyrite with giessenite; *b*, myrmekite-like tetrahedryte inclusions in galena; *c*, bismuthine rim over arsenopyrite; *d*, native gold intergrown with bismuthine; *e*, native gold intergrown with tsumoite; *f*, inclusions of tetradymite, cosalite, and native gold III in bismuthine; *g*, inclusion of native gold III in emplectite; *h*, electrum growing over native gold; *i*, inclusion of hypergene native gold V in acanthite. Apy, arsenopyrite; Ccp, chalcopyrite; Gn, galena; Ttr, tetrahedrite; Bis, bismuthine; Tsu, tsumoite; Cos, cosalite; Tmt, tetradymite; Emp, emplectite; Gies, giessenite; Elec, electrum; Acanth, acanthite; Au, native gold; Bi, native bismuth; Qz, quartz; Grt, zoned garnet crystals.

skarn formation. The oscillatory zoning suggests a complex cyclic skarn formation (repeated inflow of fluid) (Meinert et al., 2005). Garnet crystals are replaced by chlorite, hydrosericite, and carbonate.

Clinopyroxene is represented by the series diopside–hedenbergite and occurs as individual grains and their clusters measuring 0.*n* to 6 mm. Pyroxene is often replaced by carbonate and serpentine.

Chlorite is present as small green flakes forming fan-shaped clusters and chaotic segregations 0.*n* to 0.7 mm in size.

Amphibole is represented mostly by actinolite, which, together with epidote, is developed after higher-temperature skarns.

Serpentine coexists with phlogopite, actinolite, calcite, and magnetite.

Magnetite occurs as dense dissemination, nests, and granular masses mainly in the contact zones (skarns) of the Lugokan massif. The richest orebodies are localized at the exocontacts, where ores of massive structure form. In semi-oxidized ores, magnetite coexists with products of its replacement, martite (hematite) and limonite. Earlier, other researchers revealed scarce cassiterite dissemination in the near-contact zones of the Lugokan massif.

Five generations of native gold have been revealed, based on its morphology, the size and composition of its particles, and the mineral assemblages including it.

Native gold I was found as intergrowths with arsenopyrite, pyrite, and chalcopyrite and in the rock groundmass. The gold grains are rounded, irregular-shaped, interstitial, or lumpy; there are also euhedral and crystalline grains. The fineness of gold in intergrowths with arsenopyrite and pyrite varies from 890 to 950‰ (Cu ≤ 0.1%). The fineness of gold intergrown with chalcopyrite and present as inclusions in it is 900–920‰ (Hg ≤ 0.4%). According to the generally accepted classification (Petrovskaya, 1973; Nikolaeva and Yablokova, 2007), most of the native-gold shows are ultrafine-grained (50–100 μm) and fine-grained (100–250 μm).

Native gold II (single findings) is intergrown with galena and fahlore and has a fineness of 750–820‰ (SEM data).

Native gold III is found as intergrowths and as inclusions in Bi-containing minerals: bismuthine (Fig. 7d), tsumoite (Fig. 7e), cosalite (Fig. 7f), tetradymite, ingodite, emplectite (Fig. 7g), wittichenite, and giessenite. Its fineness varies from 800 to 940‰ (Cu ≤ 0.1%). The gold grains are round, irregular-shaped, interstitial, lumpy, euhedral, wire-like, and crystalline. By size, most of the native-gold shows are classified as dust-like (10–60 μm).

Native gold IV of low fineness (electrum) was found in oxidized ores from the deposit surface. Its grains are 10 to 100 μm in size; most of them are classified as dust-like and ultrafine-grained. This gold occurs as vein–lamellar, fractured, interstitial, and wire-like segregations. Its shape is reflective of the mostly limited growth space. This morphology is typical of ore occurrences of near-surface genesis (Savva and Preis, 1990). A specific compositional feature of native gold IV is a high content of Ag, which makes it silvery (white). The fineness of electrum is 400–660‰, with a distribution mode of 400–500‰. All native-gold grains have an Hg impurity (up to 2%). In addition to high-Hg electrum, high-Hg kustelite and weishanite (a natural gold amalgam) were found. The single gold grains have a zonal structure; the cores are composed of native gold of higher fineness (680‰, SEM data), and the rims, of electrum (Fig. 7h) (Redin et al., 2014). Hg-containing electrum, kustelite, and weishanite are typical of deposits formed under low sulfur fugacity conditions (f_{S_2}) (Spiridonov, 2010).

Native gold V occurs as individual moss-like grains in acanthite and has a fineness of 700–900‰ (SEM data) (Fig. 7h). In our opinion, it formed during a hypergene process.

Molybdenite is present as scales, plates, and their clusters mostly in silicified and K-feldspathized granodiorite-porphyry. The highest contents of molybdenite are typical of the central zone of the deposit, where it is disseminated, along with scheelite, in quartz veins. Molybdenite and scheelite do not occur in commercially significant amounts.

Arsenopyrite is one of the earliest sulfide minerals; it occurs as isometric and prismatic crystals with a rhombic section, intergrowths of irregular shape, and dissemination and also forms nests and veinlets (Fig. 7a). The sheared arsenopyrite crystals are cemented with later sulfides: chalcopyrite, galena, sphalerite, etc. Arsenopyrite has a nonstoichiometric chemical composition and is enriched in As (As/S > 1). The main impurities in the mineral are (wt.%) Sb (0.4), Ni (0.1), Co (0.1), and Au (0.1).

Pyrite is one of the most abundant ore minerals. It occurs as single crystals, intergrowths, and granular aggregates and is associated mainly with almost coeval arsenopyrite and chalcopyrite. Older pyrite is also found. In addition, pyrite is present as veinlets and dissemination in brecciated marbleized limestones in crush zones.

Chalcopyrite occurs as monomineral clusters, dissemination, and veinlets mostly in skarns. In quartz veins, chalcopyrite cements earlier formed pyrite. Chalcopyrite crystals are often sheared and contain later formed sulfides in cracks and interstices. Chalcopyrite also contains sphalerite, an exsolution product. The presence of stellar products of sphalerite exsolution in chalcopyrite typically indicates the high-temperature formation of the latter (Ramdohr, 1960). Seldom, intergrowths of chalcopyrite with bornite are present. Bornite contains chalcopyrite (an exsolution product) as reticulate and thin elongate tablets.

Pyrrhotite is intergrown with chalcopyrite and is also present as irregular-shaped aggregates in skarns. It is often replaced by marcasite.

Galena is minor and occurs mostly as intergrowths with sphalerite and fahlore in brecciated rocks. The main impurities are (wt.%) Ag (3), Sb (2), Bi (8), Cu (0.4), and Se (0.13).

Sphalerite has irregular-shaped grains and, together with galena, is observed in microcracks in arsenopyrite, pyrite, and chalcopyrite.

Fahlore in the studied samples is represented by tetrahedryte and tennantite. Tetrahedryte (Pb = 1, Sb = 30, Zn = 3, Cu = 34, Fe = 3, Ag = 3, and S = 24 wt.%) and tennantite (Sb = 21, As = 6, Zn = 4, Cu = 37, Fe = 4, Ag = 3, and S = 25 wt.%) occur as myrmekite-like inclusions in galena (Fig. 7b), microveinlets in chalcopyrite, and irregular-shaped aggregates and xenomorphic grains in non-ore mass. Usually, fahlore fills microcracks in earlier formed sulfides (chalcopyrite, arsenopyrite, and pyrite).

Bismuth minerals (and Bi-containing minerals) of the deposit are native bismuth, sulfides, tellurides, and sulfotellurides of Bi, and sulfosalts of various compositions (containing Bi, Cu, and Pb). Bismuth tellurides and sulfotellurides and Cu–Bi sulfosalts are localized mainly in pyroxene–garnet, garnet, garnet–phlogopite, and phlogopite–garnet skarns. They occur as scarce dissemination, nests, and microveinlets both in skarns and in cutting

quartz–carbonate veins and veinlets. Pb–Bi and Cu–Pb–Bi–S,Se sulfosalts are present mostly in quartz–carbonate–adularia and quartz–carbonate–fluorite veins.

Native bismuth is found as irregular-shaped grains both in the cracks and interstices of arsenopyrite and in skarns.

Bismuthine is one of the most abundant bismuth minerals and is present mainly as dissemination, nests, and microveinlets in skarns. It has round, sheaf-like, and acicular crystals and forms aggregates of irregular shape, rims (Fig. 7c), and fine-crystalline segregations in the cracks and interstices of arsenopyrite. Bismuthine also contains hessite, friedrichite(?), tetradymite, ingodite, emplectite, and native gold III as inclusions and intergrowths (Fig. 7d) as well as impurities of (wt.%) Pb (5), Sb (0.7), Cu (0.4), Ag (0.3), and Se (1.4).

Bismuth tellurides and sulfotellurides are represented by tsumoite, tetradymite, and ingodite. Tsumoite occurs as tabular crystals and irregular-shaped aggregates in assemblage with bismuthine, ingodite, cosalite, and native gold III (Fig. 7e). Tetradymite is one of the most abundant Bi sulfotellurides. Together with ingodite and native gold III it is present as inclusions in bismuthine (Fig. 7f).

Copper–bismuth sulfosalts are represented by wittichenite and emplectite and are typical of skarns with early Cu mineralization. Emplectite dominates over wittichenite in ores and occurs as irregular-shaped aggregates. It is often intergrown with bismuthine and contains inclusions of native gold III (Fig. 7g) and friedrichite(?) and impurities of (wt.%) Te (0.86), Pb (3.23), Fe (2.68), Sb (0.86), and Se (0.26). Wittichenite, like emplectite, forms irregular-shaped aggregates and is of limited occurrence. It contains inclusions of native gold III.

Lead–bismuth sulfosalts are represented by giessenite, kobellite, cosalite, and aschamalmite(?). Giessenite is the most abundant mineral among Pb–Bi sulfosalts. It occurs as long prismatic and acicular crystals in quartz and as xenomorphic segregations in the cracks and interstices of arsenopyrite and chalcopyrite. The studied giessenites differ slightly in the contents of major components (Bi and Pb). They contain impurities of (wt.%) Sb (9.74), Cu (2.72), Se (0.3), and Ag (1.28). Kobellite is macroscopically indistinguishable from giessenite and is identified only by electron microprobing. Some of the sulfosalts studied earlier by SEM (aschamalmite and nuffieldite) were not reliably identified, because they were extremely small and were intergrown with other minerals. They are likely to be giessenite, judging from similar composition and optical properties and the coexistence with this mineral in the samples. Cosalite is extremely rare and occurs as dissemination in skarns. It is intergrown with bismuthine, tetradymite, and native gold III and contains only impurities of Ag (up to 2%).

Pekoite and friedrichite(?) are Cu–Pb–Bi–S,Se sulfosalts (minerals of the aikinite group), which are extremely rare. Pekoite has irregular-shaped crystals. Friedrichite(?) (single findings), together with native gold III, was discovered as inclusions in bismuthine. Single schirmerite(?) (Ag–Bi sulfosalt) grains are also rare.

Antimonite was earlier found in heaps as sporadic nests and dissemination in oxidized rocks. Single cinnabar grains were found in the surface rocks of the deposit.

Hypergene mineralization is characterized by a great diversity of mineral phases. The most common minerals are malachite, azurite, iron hydroxides, and scorodite. Bornite, chalcocite, covellite, and cuprite form in the zone of secondary sulfide enrichment as a result of the replacement of chalcopyrite. Malachite and azurite result mostly from the replacement of chalcopyrite and, more seldom, fahlore. Native copper is present as inclusions in iron hydroxides, in assemblage with malachite and azurite. It contains an impurity of Sn (up to 15%, SEM data). Scorodite is developed after arsenopyrite. Iron hydroxides form earthy sinter aggregates and solid compact masses.

Hypergene Ag mineralization. In the hypergenesis zone, destruction of silver-containing mineral phases (Ag-fahlores, galena, hessite, etc.) gave rise to acanthite, chlorargyrite, I-containing argyrite, and native silver. Acanthite is found as rhythmic and moss-like segregations. It is one of the typical hypergene minerals of the oxidation zone and forms through the replacement of Ag-containing fahlores and other Ag-containing minerals. Chlorargyrite occurs as waxy, reniform, and rhythmic segregations and as moss-like outgrowths on acanthite. Iodine-containing argyrite forms irregular-shaped aggregates in the central parts of rhythmic chlorargyrite segregations. Hypergene native silver is also found as moss-like segregations in acanthite. Seldom, mckinstryite ((Ag, Cu)$_2$S) is present as replacement rims over chalcopyrite.

Sequence of ore formation. The results of study of structure–texture relationships of minerals and mineral assemblages in the main types of ores of the Lugokanskoe deposit made it possible to recognize five successive stages of mineral formation: pre-ore (I), early ore (II), ore (productive) (III), late ore (IV), and hypergenesis (V). The idealized scheme of the sequence of mineral formation is presented in Fig. 8.

The pre-ore stage is the appearance of products of high-temperature transformations of the host rocks caused by the intrusion of granodiorite-porphyry of the Shakhtama complex. These are olivine skarns (sometimes, with spinel) that formed in the near-contact zone of the Lugokan massif and are now preserved only as relics.

At the early ore stage with a temperature decrease, pyroxene–garnet, garnet, phlogopite–garnet, and phlogopite skarns with magnetite mineralization formed (the progressive stage of skarn formation). Most of magnetite with chlorite, actinolite, epidote, serpentine, calcite, and quartz formed at the retrograde stage. At the same stage, local quartz–K-feldspar zones (veins) with molybdenite and scheelite (quartz–scheelite–molybdenite mineral assemblage) formed in the central part of the massif. The early ore stage ended with the beginning of the formation of the main productive mineral assemblage (pyrite–chalcopyrite–arsenopyrite).

Mineral	Stage				
	Pre-ore	Early ore	Ore (productive)	Late ore	Hyper-genesis
Olivine					
Spinel					
Pyroxene					
Garnet					
Phlogopit					
Serpentine					
Amphibole					
Epidote					
Chlorite					
Calcite					
Quartz					
K–Na-feldspar					
Sericite					
Fluorite					
Magnetite					
Molybdenite					
Pyrite					
Pyrrhotine					
Chalcopyrite					
Arsenopyrite					
Galena					
Sphalerite					
Fahlores					
Bismuthine					
Bi tellurides					
Bi sulfotellurides					
Cu–Bi sulfosalts					
Pb–Bi sulfosalts					
Native Au			I	II III	IV V
Kustelite					
Native Ag					
Native Cu					
Acanthite					
Argyrite					
Malachite					
Azurite					
Fe hydroxides					

Fig. 8. Sequence of mineral formation. I–V, native-gold generations.

Three mineral assemblages formed at the ore (productive) stage: gold–pyrite–chalcopyrite–arsenopyrite, gold–polymetallic, and gold–bismuth. The gold–pyrite–chalcopyrite–arsenopyrite assemblage is found mainly at the endo- and exocontacts of the Lugokan massif; it is present as dissemination and nests and in quartz–carbonate veins and veinlets in skarns. This assemblage is specific to sericitization and silicification zones. An early gold-including mineral assemblage is also revealed in the marbleized limestones of the Bystraya Formation; it is observed as quartz–carbonate–sericite veinlets in crush zones. The study of the mineral composition has shown several major types of ores with varying contents of the main minerals: pyrite–pyrrhotite–chalcopyrite, pyrite–arsenopyrite, pyrite–chalcopyrite–arsenopyrite, and pyrite.

Gold–polymetallic mineral assemblage is of limited occurrence and is superposed on the earlier formed sulfide ores (gold–pyrite–chalcopyrite–arsenopyrite assemblage). It was found in the brecciation and shearing zones. Sulfide minerals of this assemblage are localized mainly in the cracks of

earlier formed sulfides (pyrite, arsenopyrite, and chalcopy-rite), which indicates its later formation relative to the gold–pyrite–chalcopyrite–arsenopyrite assemblage.

Gold–bismuth mineral assemblage is the latest and is su-perposed on the earlier formed sulfide ores (gold–pyrite–chalcopyrite–arsenopyrite and gold–polymetallic mineral assemblages). It is found in skarns and in quartz–carbon-ate–adularia and quartz–carbonate–fluorite veinlets and veins in the crush zones of limestones. In skarns, gold–bis-muth mineralization is usually localized in brecciation zones and cutting quartz–carbonate veins and veinlets.

The late ore stage was recognized arbitrarily. At this stage, a gold–silver mineral assemblage formed, which was found only in the samples from the deposit surface. There-fore, we assume that low-fineness native gold (electrum), kustelite, and weishanite might have formed during later hy-pergene processes.

After the completion of the hydrothermal process, the de-posit ores underwent hypergene transformations (hypergen-esis stage), which are expressed in the appearance of clay minerals, iron hydroxides, and other hypergene minerals (malachite, azurite, scorodite, etc.) widespread at the depos-it surface. The degree of ore oxidation varies in orebodies and generally decreases downsection.

RESULTS OF STUDY OF FLUID INCLUSIONS

For study of fluid inclusions we sampled ore-bearing quartz and quartz–carbonate veins from several productive gold mineral assemblages of the Lugokanskoe deposit. Fluid inclusions (FI) were examined in quartz and carbonate of native-gold (I)–pyrite–chalcopyrite–arsenopyrite assem-blage, chalcopyrite-containing gold–polymetallic mineral assemblage (2), and gold–bismuth mineral assemblage spread in skarns (3) and limestone crush zones (4).

Primary, primary–secondary, and secondary FI measur-ing 4 to 45 μm (on average, 10–25 μm) were found in the polished transparent plates. Some secondary FI reach 100–130 μm in size. According to optical observations, the FI are subdivided into three main types according to the phase ra-tio at room temperature (Fig. 9):

type I—essentially gas FI containing mainly a gas phase and a small amount of salt solution (Fig. 9*a*);

type II—two-phase FI containing a salt solution and a minor gas phase as a bubble (which might contain ore sub-stance particles) (Fig. 9*b, d, g*);

type III—multiphase FI containing a salt solution, a gas phase, an isotropic cubic salt crystal (probably, halite (NaCl)), and, sometimes, an ore phase (Fig. 9*c, e, f, h*).

Primary FI are localized singly or in groups in the cores and along the growth zones of quartz or calcite crystals. In-clusions can be evenly distributed throughout grains of vein minerals. The inclusion vacuole is isometric, specific to a negative crystal, elongate, and, seldom, irregular-shaped. Secondary FI have irregular-shaped vacuoles; they are lo-calized in groups in the healed microcracks of quartz and quartz–calcite veinlets and are often subject to "unlacing" (Roedder, 1984). The inclusions concentrated in the cracks of quartz and calcite crystals healed during their growth are primary–secondary, with isometric elongate vacuoles. For FI study we used primary and primary–secondary FI respon-sible for the ore genesis in the Lugokanskoe deposit.

Quartz from productive veins of ore mineral assemblage (1) of the Lugokanskoe deposit contains FI of three types. Primary FI of type II (Fig. 9*b*) are homogenized into a liquid phase at temperatures (T_{hom}) of 300–390 °C (Table 2). The eutectic temperatures (T_{eut}) range from –40 to –37 °C, and the temperature of ice melting (T_{melt}) is –20 to –12 °C. Thus, the concentration of salts in the solutions of primary type II FI is estimated at 16.0–22.6 wt.% NaCl-equiv (Fig. 10), and

Table 2. Results of heating and cooling of FI in the minerals of the Lugokanskoe deposit

Type of mine-ralization	Mineral	Type of FI	Kind of FI	n	T_{hom}, °C	T_{eut}, °C	T_{melt}, °C	$T_{melt.sol}$, °C	C_{salt}, wt.% NaCl equiv.	*Salt composition of solution
1	Quartz	I	P	11	N.d.	N.d.	–48 to –45 –96 to –86	N.d.	N.d.	N.d.
	Quartz ›	II	P	45	300–390	–40 to –37	–20 to –12	N.d.	16.0–22.6	Na, Fe, K, and Mg chlorides
	Quartz ›	III	P	35	290–380	N.d.	N.d.	280–370	38–43	N.d.
2	Quartz	II	P–S	42	320–350	–25 to –21	–11 to –7	N.d.	10.5–15.0	Na and K chlorides
	Quartz	II	P	48	225–290	–27 to –25	–18.5 to –7.7	N.d.	11.4–21.5	Na and Fe chlorides
	Quartz	III	P	26	250–270	N.d.	N.d.	240–255	35–36	N.d.
3	Quartz	II	P	30	200–295	–38 to –36	–4.5 to –1.5	N.d.	2.5–7.1	Na, K, Mg, and Fe chlorides
	Calcite	II	P	30	230–330	–38 to –36	–3.8 to –2.4	N.d.	3.6–6.2	Na, K, Mg, and Fe chlorides
4	Quartz	II	P	52	170–220	N.d.	–8 to –4(2)	N.d.	(3.3)6.4–11.7	N.d.

Note. Here and in Table 3: 1, quartz veins with ore mineral assemblage (1); 2, quartz veins (2); 3, quartz–carbonate veins among skarns (3); 4, quartz–carbon-ate–adularia veins (4); N.d., not determined; P, primary FI; P–S, primary–secondary FI; n, number of measured FI; $T_{melt.sol}$, temperature of solid phase melting. *The salt composition of solution was determined after Borisenko (1982).
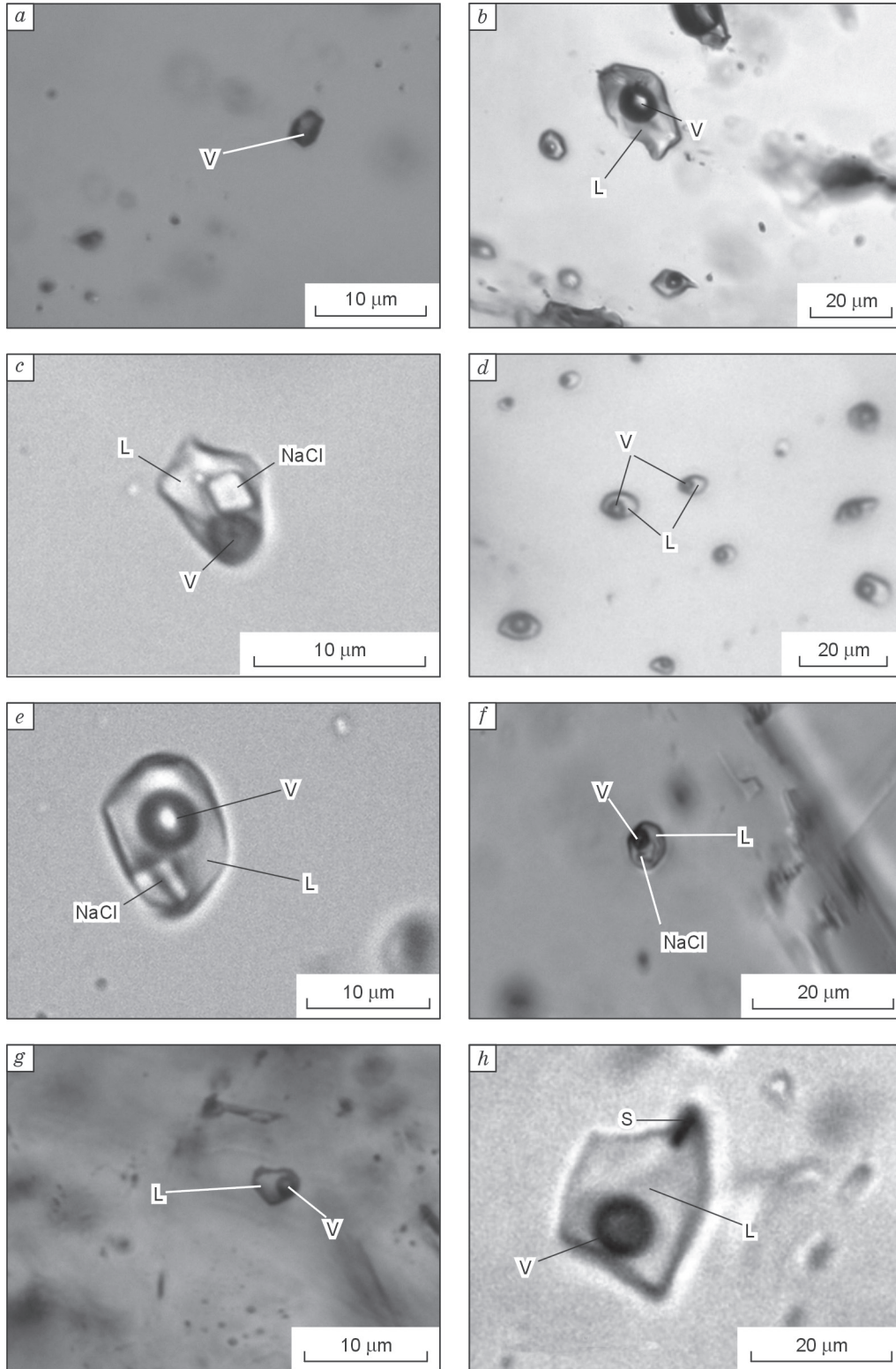
Fig. 9. Primary fluid inclusions from the Lugokanskoe deposit. *a*, Essentially gas FI in quartz of ore mineralization (1); *b*, two-phase FI in quartz (1); *c*, multiphase FI with NaCl crystals in quartz (1); *d*, two-phase FI in quartz (2); *e*, three-phase FI with NaCl crystal in quartz (2); *f*, three-phase FI with NaCl crystal in calcite (3); *g*, two-phase FI in quartz (3); *h*, two-phase FI with an ore phase in quartz (4). Parenthesized numerals mark the type of mineralization. V, gas phase; L, liquid phase; S, solid phase.
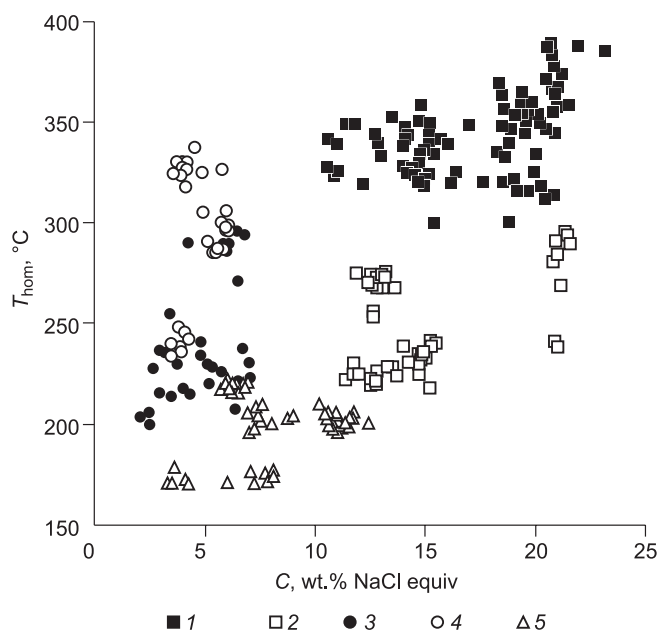
Fig. 10. Homogenization temperatures and concentrations of solutions of type II FI from different mineral assemblages of the Lugokanskoe deposit (microthermometry data). *1*, primary and pseudosecondary FI in quartz veins of ore mineral assemblage (1); *2*, FI in quartz veins (2); *3*, FI in quartz (3); *4*, FI in carbonate (3); *5*, FI in quartz–carbonate–adularia veins (4).

the solutions of the studied FI contain not only NaCl but also chlorides of Fe, K, and Mg (Borisenko, 1982) (Table 2). According to the Raman spectroscopy data, the gas phase of primary gas–liquid inclusions of type II contains a mixture of CO_2 and N_2, with the former prevailing. The content of N_2 in the gas phase reaches 26 vol.% (Table 3). The primary–secondary FI of type II have similar temperatures of homogenization into a liquid phase, 320–350 ℃, and the eutectic and ice melting temperatures are –25 to –21 and –11 to –7 ℃, respectively. The concentration of salts in these inclusions is estimated at 10.5–15.0 wt.% NaCl-equiv (Fig. 10). The salt solution of the inclusions contains a mixture of Na and K chlorides, and the gas phase contains CO_2 (Tables 2 and 3). The temperature of homogenization of CO_2 into a gas phase in the fluid is –48 to –45 ℃, and the temperature of complete homogenization of the FI is 320–350 ℃. According to the FLINCOR program data (for the system CO_2–H_2O), the density of CO_2 in the fluid phase is ~0.02 g/cm^3, which corresponds to a pressure of 900–1500 bars.

Primary FI of type III (Fig. 9c) from quartz veins (1) are characterized by high temperatures of homogenization (into a liquid phase), 290–380 ℃, and the temperature of NaCl melting is 280–370 ℃ ($T_{sol.melt}$), which corresponds to the salt concentration of 38–43 wt.% NaCl-equiv (Table 2). Primary FI of type III contain a CO_2–N_2 mixture in the gas phase, with a predominance of N_2, up to the complete absence of CO_2 (Table 3). Small opaque ore mineral phases are sometimes identified in the FI of types II and III.

Fluid inclusions of type I (essentially gas FI) (Fig. 9a) are often localized together with FI of types II and III (gas–liquid and crystal–fluid inclusions), which suggests the heterogeneous state of the fluid system at the moment of FI trapping (Kovalenker et al., 2011; Prokof'ev et al., 2012; Nikolaev et al., 2014). They are primary or primary–secondary inclusions. According to Raman spectroscopy data, the type I inclusions have a $CO_2 \pm N_2$ gas phase (Table 3). Thus, the presence of ores in the early gold mineral assemblage (1) of the Lugokanskoe deposit was controlled by fluids containing chlorides of Na, K, Fe, and Mg in the solution and CO_2 and N_2 in the gas phase.

We revealed FI of three types in quartz with ore mineralization (2). In contrast to the FI from quartz of early gold mineral assemblage (1), the primary FI of type II of gold–polymetallic mineralization (Fig. 9d) are characterized by rather low temperatures of homogenization (into a liquid phase), 225–290 ℃ (Table 2). The eutectic temperature of gas–liquid inclusions is –27 to –25 ℃, and the temperature of ice melting is –18.5 to –7.7 ℃. Thus, the salt phase in the solution of type II FI is a mixture of Na and Fe chlorides (Borisenko, 1982); the concentration of salts varies from 11.4 to 21.5 wt.% NaCl-equiv (Fig. 10). Primary FI of type III (Fig. 9e) are homogenized (into a liquid phase) at 250–270 ℃; the temperature of dissolution of the solid phase (halite) is 240–255 ℃, which indicates that the salt concentration in the solution is 35–36 wt.% NaCl-equiv (Table 2). According to the Raman spectroscopy data, gas–liquid (type II) and crystal–fluid (type III) inclusions in the gas phase contain CO_2. The temperature of homogenization of CO_2 (into a gas phase) of gas–liquid inclusions is –56 to –51 ℃, which corresponds to a CO_2 density of ~0.017 g/cm^3 and a pressure of 650–750 bars.

Gold–bismuth mineral assemblage was found in quartz–carbonate veinlets containing bismuthine, tetradymite, tsumoite, ingodite, and native gold III (3) in skarns and in quartz–carbonate–adularia veinlets containing giessenite and kobellite (4) in the crush zones of limestones. Quartz–carbonate veinlets (3) contain mainly primary two-phase gas–liquid inclusions. Primary FI of type II in quartz (Fig. 9g) are characterized by medium temperatures of homogenization (into a liquid phase), 200–295 ℃, and primary FI of type II in calcite, by $T_{hom} = 230–330$ ℃ (Table 2). The eutectic temperatures of gas–liquid inclusions in quartz and carbonate are –38 to –36 ℃, and the temperatures of ice melting are –4.5 to –1.5 ℃ and –3.8 to –2.4 ℃, respectively, which corresponds to a low concentration of salts in the solutions, 2.5–7.1 wt.% NaCl-equiv (Fig. 10). The salt phase is a mixture of Na, K, Mg, and Fe chlorides (Table 2). Along with type II FI, there are essentially gas and three-phase FI (with a halite cube) in calcite (Fig. 9f), which suggests a heterogeneous trapping of fluids, as noted above. Raman spectroscopy revealed CO_2 gas in the type II FI (Table 3). The FI studies of these samples encountered difficulty, because calcite crystals often cracked along the cleavage planes on strong cooling or heating.

Table 3. Raman spectroscopy data on the composition of the gas phase of inclusions in the minerals of the Lugokanskoe deposit

Type of mineral-ization	Host mineral	Type of FI	Kind of FI	CO_2	N_2	H_2O
				vol.%		
		I	P	85.4	14.6	Traces
		I	P	100	N.d.	Traces
		II	P	76	24	Traces
		II	P	79.3	20.7	Traces
		II	P	74	26	Traces
		II	P–S	100	N.d.	Traces
1	Quartz	II	P–S	100	N.d.	Traces
		II	P–S	100	N.d.	Traces
		II	P–S	100	N.d.	Traces
		II	P–S	100	N.d.	Traces
		II	P–S	100	N.d.	Traces
		III	P	14	86	Traces
		III	P	N.d.	100	Traces
		I	P	100	N.d.	Traces
		II	P	100	N.d.	Traces
		II	P	100	N.d.	Traces
2	Quartz	III	P	100	N.d.	Traces
		III	P	100	N.d.	Traces
		III	P	100	N.d.	Traces
		III	P	100	N.d.	Traces
3	Quartz	II	P	100	N.d.	Traces
		II	P	100	N.d.	Traces
		II	P	100	N.d.	Traces
4	Quartz	II	P	100	N.d.	Traces
		II	P	N.d.	N.d.	100
		II	P	N.d.	N.d.	100

Note. Gases CH_4, NH_3, and H_2S were not detected.

For type II FI from quartz–carbonate–adularia veinlets (4), the temperatures of homogenization (into a liquid phase) are 170–220 ºC, the temperatures of ice melting are –8 to –4 (–2) ºC, and the salt concentrations are 3.3–11.7 wt.% NaCl-equiv (Table 2, Fig. 10). Seldom, gas–liquid FI containing an opaque acicular ore mineral are present (Fig. 9h).

Secondary inclusions from the studied mineral assemblages are gas–liquid and essentially gas fluids with different variations in CO_{2g} and water vapor contents in the gas phase. The FI studies of secondary inclusions are complicated by their small sizes. The decrepitation temperatures of late FI are within 50–85 ºC; therefore, we failed to obtain reliable information about the parameters of secondary hydrothermal and metasomatic processes of transformation of ore parageneses in the Lugokanskoe deposit.

RESULTS OF ISOTOPE-GEOCHRONOLOGICAL STUDIES

A crucial problem of the genesis of gold deposits in eastern Transbaikalia is the determination of the age of gold mineralization, which is the basis for its correlation with magmatism and for analysis of the metallogeny of gold in eastern Transbaikalia. In the review of the metallogeny of Central Asia (Goldfarb et al., 2014), the Lugokanskoe deposit is dated at the Early Cretaceous. According to other data, the K–Ar age of hydrothermal rocks of the Lugokanskoe deposit is 157–132 Ma (Sazonov, 1978). Our studies of the $^{40}Ar/^{39}Ar$ age of K-containing minerals of syn-ore parageneses by the stepwise-heating technique described earlier (Travin et al., 2009) have shown that gold mineralization formed within the Lugokan ore cluster in the Late Jurassic: The age of early gold–pyrite–chalcopyrite–arsenopyrite assemblage is 160 ± 2 Ma, and the age of gold–bismuth mineralization is 155.9 ± 4.5 Ma (Redin et al., 2015). The obtained age spectra (Fig. 11) can be interpreted as undisturbed or weakly disturbed. All spectra have a plateau matching the required criteria (Fleck et al., 1977). The estimated age of granodiorite-porphyry of the Lugokan massif does not contradict the age determined on phlogopite from chalcopyrite-containing phlogopite skarns. The difference in the age plateaus does not exceed δ = 2.7 and, correspondingly, is not significant.
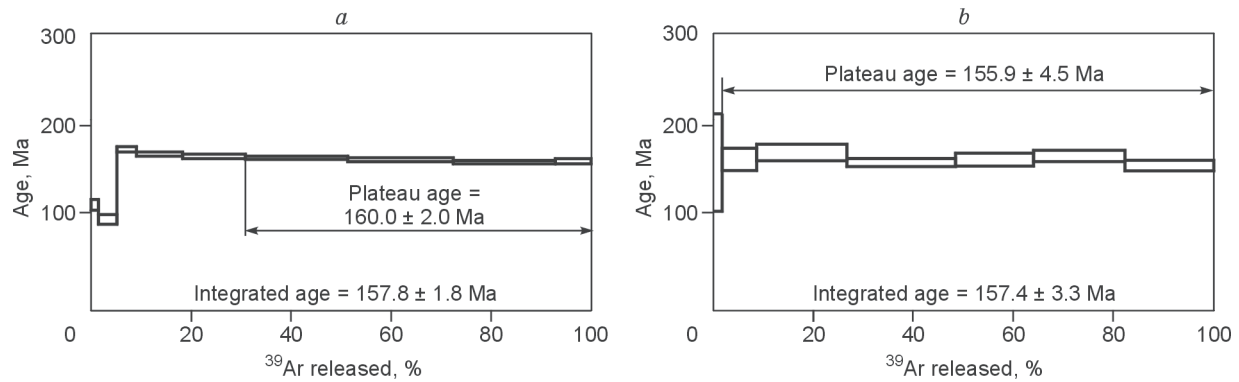
Fig. 11. Ar–Ar age plateaus. *a*, Phlogopite; *b,* adularia *(*Redin et al., 2015).

The isotopic composition of sulfur in most of sulfide minerals (Table 4) is rather homogeneous and varies from 2.5 to 6.6‰.

The results of our study of the isotopic composition of C and O are given in Table 4. The host limestones have $\delta^{13}C$ = 5.1 and 6.0‰ and $\delta^{18}O$ = 8.1 and 10.1‰. For coarse-crystalline calcite from recrystallized limestone, a similar $\delta^{13}C$ value (4.3‰) but a strongly different $\delta^{18}O$ value (–1.0‰) were obtained. The $\delta^{13}C$ and $\delta^{18}O$ values of carbonate of mineralized veins in the Lugokanskoe deposit form two modes. The first mode, with negative $\delta^{13}C$ values (–6.6 to –4.6‰) and high $\delta^{18}O$ values (13.5–14.5‰), is specific to quartz–carbonate rocks with pyrite, arsenopyrite, chalcopyrite and native gold I. The second mode, with high $\delta^{13}C$ values (2.7–3.4‰) and medium $\delta^{18}O$ values (6.4–6.8‰), is typical of quartz–carbonate veinlets containing bismuthine, tetradymite, tsumoite, ingodite, and native gold III. Abnormal $\delta^{18}O$ values were obtained for carbonate of quartz–carbonate–adularia and quartz–carbonate–fluorite veinlets containing giessenite and kobellite, 0.1 and –2.3‰, respectively.

DISCUSSION

The obtained new geological, petrographic, petrochemical, mineralogical, geochemical, isotope-geochronological, and physicochemical data make it possible to clarify the genesis of the Lugokanskoe deposit. Comparison of these data with data on other intrusion-related gold systems (IRGS) shows that the main parameters of the Lugokanskoe deposit are convergent with those of reduced porphyry copper–gold deposits (RPCGD) and reduced (RIRGS) (Table 5).

One of the main factors affecting the localization and specifics of gold mineralization in IRGS is the chemical composition of magma and the degree of its oxidation (Hart et al., 2000). By petrochemical and geochemical parameters, the igneous rocks of the Shakhtama complex at the Lugokanskoe and Serebryanoe deposits belong to type I granitoids. The low Fe_2O_3/FeO ratios (<0.5) and the presence of ilmenite (and, less, magnetite) among the accessory minerals give grounds to assign the igneous rocks of the Shakhtama complex of the Lugokanskoe deposit to the ilmenite (re-

duced) series, which is absolutely atypical of porphyry Au–Cu–Mo deposits spatially and genetically related to oxidized intrusions.

Table 4. Isotopic compositions of S, O, and C in the ore minerals of the Lugokanskoe deposit

No.	Mineral	$\delta^{34}S$, ‰	$\delta^{13}C$, ‰	$\delta^{18}O$, ‰	Reference
1	Pyrite	2.5	N.d.	N.d.	(Redin et al., 2015)
2	Arsenopyrite	3.0	N.d.	N.d.	(Redin et al., 2015)
3	Chalcopyrite	3.8	N.d.	N.d.	(Redin et al., 2015)
4	Chalcopyrite	4.1	N.d.	N.d.	(Redin et al., 2015)
5	Bismuthine	6.6	N.d.	N.d.	(Redin et al., 2015)
6	Arsenopyrite	5.7	N.d.	N.d.	Our data
7	Chalcopyrite	2.8	N.d.	N.d.	Our data
8	Carbonate	N.d.	5.1	8.1	Our data
9	Carbonate	N.d.	6	10.1	Our data
10	Carbonate	N.d.	4.3	–1.0	Our data
11	Carbonate	N.d.	–5.6	14.5	Our data
12	Carbonate	N.d.	–5.1	14.1	Our data
13	Carbonate	N.d.	2.7	6.4	Our data
14	Carbonate	N.d.	2.8	6.8	Our data
15	Carbonate	N.d.	–6.6	13.8	Our data
16	Carbonate	N.d.	3.4	0.1	Our data
17	Carbonate	N.d.	2.8	–2.3	Our data
18	Carbonate	N.d.	–4.6	13.5	Our data

Note. 1, dissemination in quartz–sericite veinlets of crush zone in limestones; 2, quartz veinlets in skarns; 3, dissemination in skarns; 4, dissemination in quartz–carbonate veinlets in skarns; 5, dissemination in quartz–carbonate veinlets and skarns; 6, quartz veins and veinlets of crush zone in marbleized limestones; 7, dissemination in skarns; 8, 9, marbleized limestone;10, coarse-crystalline calcite from recrystallized limestone; 11, quartz–carbonate nests and veinlets containing pyrite, arsenopyrite, chalcopyrite, and native gold I in skarns; 12, carbonate veins containing chalcopyrite and pyrite in skarns; 13, quartz–carbonate veinlets containing bismuthine, tetradymite, and native gold III in garnet skarns; 14, quartz–carbonate veinlets containing bismuthine, tetradymite, tsumoite, ingodite, and native gold III in garnet skarns; 15, quartz–carbonate veinlets containing arsenopyrite and chalcopyrite in garnet skarns; 16, quartz–carbonate–adularia veins containing giessenite and kobellite; 17, quartz–carbonate–fluorite veinlets and veins containing giessenite in brecciated limestone; 18, crush zone with pyrite, arsenopyrite, and chalcopyrite in quartz–K-feldspar rock. N.d., not determined.

Table 5. Comparative analysis of the identification features of the Lugokanskoe deposit, RIRGS, and RPCG

Identification criteria	Reduced intrusion-related gold systems (Hart, 2007)	Reduced porphyry copper–gold deposits (Rowins, 2000)	Lugokanskoe deposit
Reference objects	Fort Knox (Alaska), Dublin Gulch, Scheelite Dome, Clear Creek (Tombstone Gold Belt, Yukon)	Mile Hill (Australia), San Antonio (Mexico), Madeleine (Quebec), Copper Canyon (Nevada)	Lugokanskoe deposit (eastern Transbaikalia)
Geodynamic setting of formation	Collision, postcollisional extension	Subduction zones	Completion of collision
Magmatism	Reduced *I*-type and, more seldom, *S*-type metaluminous (sometimes, peraluminous) granitoids (granite–monzonite–granodiorite ones)	Reduced *I*-type granitoids with a porphyritic texture (from dioritic porphyrites to quartz granite-porphyry)	Reduced *I*-type metaluminous granitoids with a porphyritic texture (granodiorite–granite ones)
Geologic (structural) location	In large tectonic zones	In zones of intersecting deep faults	In zone of the intersecting regional Urov–Dzhalir and Budyumkan deep faults
Structure-morphological type of mineralization	Foliation veins and, more seldom, stockwork–vein orebodies within the intrusion; skarns, mineralized breccias, veins, and disseminated orebodies in the immediate vicinity of the intrusion; hydrothermal breccias, quartz–sulfide veins, and Au–Ag veins at several kilometers from the pluton	Stockwork–vein orebodies and foliation veins within the massif	Sheet-like, lenticular, and vein-like orebodies
Mineral composition	Pyrrhotite, chalcopyrite, arsenopyrite, Bi–Te–Sb–Pb–Au minerals, galena, sphalerite, and native Au	Pyrite, pyrrhotite, chalcopyrite, molybdenite, galena, sphalerite, W minerals, and native gold; no hematite, magnetite, and sulfate minerals, but much hypogene pyrrhotite	Pyrite, arsenopyrite, chalcopyrite, pyrrhotite, magnetite, Bi minerals, sphalerite, galena, fahlores, and native gold
Geochemical composition	Major components: Bi, Te, and As; subordinate components: Sb, Pb, Zn, and Ag; Au content is in direct correlation with Bi and Te contents; high Cu contents are atypical	Major components: Au, Ag, and Cu; subordinate components: Mo, Pb, Zn, and W	Major components: Au, Ag, and Cu; subordinate components: As, Bi, Pb, and Sb
Formation conditions	Fluid enriched in CO_2, with impurities of CH_4, H_2S, and N_2, weakly to moderately saline (up to 12 wt.% NaCl equiv.), of chloride composition, $T = 200$–600 °C, $P = 0.5$–30 kbar	Aqueous–chloride fluid rich in CO_2 with a permanent impurity of CH_4; $T = 150$–600 °C (250–450 °C), $P = 0.5$–2.0 kbar	Fluid enriched in CO_2, containing an impurity of N_2, concentration of salts from 5 to 19 wt.% NaCl equiv., of chloride composition, $T = 170$–390 °C, $P = 0.7$–1.5 kbar
Time of formation	Mesozoic (middle Cretaceous for Western Canada and Eastern Alaska)	Mesozoic and Cenozoic	Mesozoic (Late Jurassic)

As known from the published literature, the reducing environment is preserved during the hydrothermal-metasomatic processes of skarn formation and the following processes responsible for commercial gold mineralization (Meinert et al., 2005). At the Lugokanskoe deposit, the ore formation process began synchronously with the intrusion of granodiorite-porphyry, which resulted in olivine, pyroxene–garnet, garnet, garnet–phlogopite, phlogopite–garnet, and phlogopite skarns with magnetite mineralization. Although reduced intrusions usually provoke the formation of reduced skarns (Px >> Grt), the Lugokanskoe deposit is characterized by the formation of typical oxidized skarns (Grt >> Px) with magnetite mineralization. It is well known that the formation of oxidized or reduced skarns is related not only to the composition of the intrusion but also to the depth of its origin (Meinert et al., 2005). This dependence is clearly shown in Fig. 12. It is seen that oxidized skarns can form only when a reduced intrusion originated at shallow depths. Under these conditions, a magmatic fluid might have been mixed with meteoric waters. Commercial contents of Mo

are atypical of RIRGD. The same is true for the Lugokanskoe deposit, where molybdenite is of local occurrence (Hart et al., 2000). The presence of minor molybdenum mineralization in the Lugokanskoe deposit might be due to the initial enrichment of the Shakhtama complex granitoids in granitophile and trace elements (B, F, Li, Rb, Cs, Be, Sn, W, Mo, Nb, Ta, Th, and U) (Kozlov, 2011).

Another specific feature of RIRGD is the arrangement of orebodies relative to the pluton. As mentioned above, gold mineralization in the Lugokanskoe deposit is localized mainly in skarns and, less, carbonate rocks and granodiorite-porphyry of the Lugokan massif. Most orebodies occur subconformably with the intrusion contacts. The confinement of orebodies to skarns and their sheet-like, lenticular, or vein-like morphology are specific to deposits localized within skarn intrusions or in the immediate vicinity of them. Hart et al. (2000) assign such deposits to types I and II.

The ores of the Lugokanskoe deposit differ slightly from those of typical RIRGD: They contain much chalcopyrite in early gold mineral assemblage and are poor in tungsten mi-

neralization. This might be due to the relationship of tungsten mineralization with reduced *I*-type granitoids, which contain much more Cu and Au than *S*-type granitoids. As shown by Burnham and Ohmoto (1980), *S*-type magmas contain only about 10% of sulfur present in *I*-type granitoids and are partial melts of metasedimentary sources being much poorer in Cu and Au. A specific feature of RIRGD is a close relationship of native gold with Bi minerals, which has also been established for the Lugokanskoe deposit.

The studies of FI in ore-bearing quartz and carbonate of the Lugokanskoe deposit has shown a gradual decrease in the homogenization temperature of ore-bearing fluid in passing from early to late mineral assemblages and with a distance from the intrusion. This is evidenced from the minimum homogenization temperatures of FI in quartz–carbonate–adularia veinlets with late Au–Bi mineralization and localized beyond the endocontact of the Lugokanskoe massif. In addition, the salinity of ore-bearing fluids decreases from ~19 wt.% NaCl-equv at the early stages of the evolution of the hydrothermal ore system to ~5 wt.% NaCl-equiv at the late ones. A decrease in temperature and the fluid salinity implies dilution of the primary solution with meteoric waters during its evolution. This does not contradict the calculated pressure of mineral formation (1500–650 bars) corresponding to the hypabyssal conditions. The estimated eutectic temperatures indicate a complex composition of the salt solution, which contains Na, K, Fe, and Mg chlorides. Raman spectroscopy shows the presence of CO_2 in the gas phase of FI of all mineral assemblages. In addition, N_2 or water vapor is present. The established formation conditions of ores of the Lugokanskoe deposit (high temperatures of the beginning of the ore-forming process, fluid heterogenization, the presence of water–chloride solutions with a wide range of NaCl concentrations, and the presence of carbon dioxide in the gas phase) are specific features of deposits formed at a shallow depth (<1.5 kbar), including RIRGD (Baker and Andrew, 1991; McCoy et al., 1997; Baker and Lang, 1999, 2001; Lang et al., 2000; Rombach and Newberry, 2001).

The studies of the carbon and oxygen isotope compositions have shown that the host limestones have $\delta^{13}C$ values typical of marine limestones (2–5‰ (Hoefs, 2015)) and low $\delta^{18}O$. These values indicate that the rocks underwent intense metamorphic transformations involving a magmatic fluid (Bowman, 1998). Meteoric waters seem to have actively participated in the formation of coarse-crystalline vein calcite in the recrystallized limestone, which explains the significant lighting of the oxygen isotope composition.

The relatively light carbon isotope composition of quartz–carbonate veinlets containing pyrite, arsenopyrite, chalcopyrite, and native gold I is due to intercalates of carbonaceous shale: In the host carbonate strata, such shales are characterized by strongly negative $\delta^{13}C$ values, about –25‰ (Hoefs, 2015). The slightly lower $\delta^{18}O$ values of the veinlets relative to $\delta^{18}O \approx 21–26‰$ of the limestone units are due to
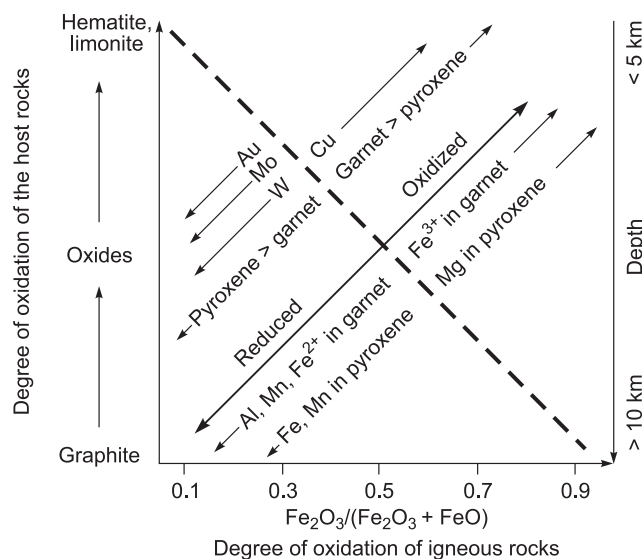
Fig. 12. Dependence of the degree of oxidation of skarn rocks on the pluton and host-rocks specifics (Meinert et al., 2005). The degree of oxidation of igneous rocks is determined by the $Fe_2O_3/(Fe_2O_3 + FeO)$ ratio. It also depends on the presence of oxides (e.g., ilmenite, magnetite, and hematite) and the iron content in dark-colored minerals, such as pyroxene, amphibole, and biotite. The degree of oxidation of the host rocks is estimated from the contents of excess carbon (e.g., graphite) sulfides (pyrrhotite and pyrite), and oxides (ilmenite, magnetite, and hematite). Approximate estimate of the depth of mineral formation: subsurface (<5 km) and great (>10 km).

the interaction with the primary fluid separated from the granite intrusion with $\delta^{18}O \approx 6–10‰$ (Hoefs, 2015).

The carbon isotope composition of quartz–carbonate veinlets containing bismuthine, tetradymite, tsumoite, ingodite, native gold III, giessenite, and kobellite varies insignificantly, which indicates a single source of carbon. This is typical of marine limestone. The lighting of the oxygen isotope composition relative to that of the limestone units is, most likely, due to the intense interaction with a magmatic fluid. The extraordinarily low $\delta^{18}O$ value of carbonate from quartz–carbonate–adularia and quartz–carbonate–fluorite veinlets containing giessenite and kobellite suggests the participation of meteoric waters in the ore formation at its final stages. This phenomenon was observed in metamorphic rocks of Transbaikalia (Izbrodin et al., 2014).

The study of the sulfur isotope composition of sulfide minerals of the Lugokanskoe deposit has shown the mantle–crust source of sulfur (Seal, 2006).

According to modern concepts, RIRGD usually form in the settings of collision and subsequent tectonic activity. Our data on the age of mineralization and igneous rocks spread within the ore cluster are in agreement with these concepts. Most of large gold deposits in eastern Transbaikalia formed in the Middle–Late Jurassic (in collision settings) and Early Cretaceous (in rifting settings) (Zorin et al., 2001). The $^{40}Ar/^{39}Ar$ dating of K-containing minerals of synore parageneses has shown that the gold mineralization of the

Lugokan ore cluster formed in the Late Jurassic (Redin et al., 2015). At the same time, the igneous rocks of the Shakhtama complex were widespread; they formed at the final stage of the collision process (Berzina et al., 2013).

The above data apparently confirm that the Lugokanskoe gold deposit is of the RIRGD type. Note that it is similar to RPCG in many features revealed during our study.

CONCLUSIONS

The Lugokanskoe Au–Cu skarn deposit is assigned to RIRGD. Gold mineralization is localized mainly in skarns and, less, in carbonate rocks (intensely transformed by tectonic processes). Sulfide ores are superposed on ore-bearing rocks (skarns). There are several varieties of skarns within the deposit: olivine, pyroxene–garnet, garnet, garnet–phlogopite, phlogopite–garnet, and phlogopite. We have established that gold–pyrite–chalcopyrite–arsenopyrite and gold–bismuth assemblages are the main productive parageneses. The study of the isotopic composition of sulfur of sulfide minerals has established its endogenous source. The $^{40}Ar/^{39}Ar$ dating of K-containing minerals of syn-ore parageneses has shown that gold mineralization within the Lugokan ore cluster formed in the Late Jurassic. At the same time, the igneous rocks of the Shakhtama complex were spread in the study area; their age corresponds to the final stage of the collision process. The obtained data on the age of the mineralization and igneous rocks of the Shakhtama complex, along with the direct geological observations, indicate their spatial, temporal, and genetic relationships. This is confirmed by the results of the study of the carbon and oxygen isotope compositions of ore-bearing veins. The igneous rocks of the Lugokan massif are metaluminous high-K ilmenite (reduced) *I*-type granitoids. The study of fluid inclusions by heating and cooling and Raman spectroscopy has shown that the mineral formation was accompanied by a gradual decrease in the content of salts in the ore-forming fluids and by a decrease in their homogenization temperatures. The optical observations have demonstrated that the fluid was heterogeneous at the early stages of the mineral formation. The evolution of the ore system was accompanied by a change in the gas phase composition of FI from predominantly nitrogen–carbon dioxide to essentially aqueous, with a carbon dioxide impurity ($H_2O + CO_2 \pm N_2 \rightarrow H_2O \pm CO_2$). The research data testify to the magmatic nature of fluids and the participation of meteoric waters at the late stages of the ore-forming process.

REFERENCES

Abramov, B.N., 2012. Formation conditions and mineralogical and geochemical compositions of rocks and ores of the Middle Golgotai gold deposit (eastern Transbaikalia). Izvestiya Vuzov. Geologiya i Razvedka, No. 3, 79–82.

Arzamastsev, A.A., Fedotov, Zh.A., Arzamastseva, L.V., Travin, A.V., 2010. Paleozoic tholeiite magmatism in the Kola igneous province: Spatial distribution, age, relations with alkaline magmatism. Dokl. Earth Sci. 430 (2), 205–209.

Baker, E.M., Andrew, A.S., 1991. Geologic, fluid inclusion, and stable isotope studies of the gold-bearing breccia pipe at Kidston, Queensland, Australia. Econ. Geol. 86, 810–830.

Baker, T., Lang, J.R., 1999. Geochemistry of hydrothermal fluids associated with intrusion-hosted gold mineralization, Yukon Territory, in: Mineral Deposits: processes to processing: Proceedings of the Fifth Biennial SGA Meeting and Tenth Quadrennial IA GOD Symposium, London, United Kingdom, 22–25 August 1999. Balkema, Rotterdam, pp. 17–20.

Baker, T., Lang, J.R., 2001. Fluid inclusion characteristics of intrusion-related gold mineralization, Tombstone–Tungsten magmatic belt, Yukon Territory, Canada. Mineral. Deposita 36, 563–582.

Bakke, A.A., 1995. The Fort Knox "porphyry" gold deposit—Structurally controlled stockwork and shear quartz vein, sulphide-poor mineralization hosted by Late Cretaceous pluton, east–central Alaska, in: Schroeter, T.A. (Ed.), Porphyry Deposits of Northwestern Cordillera of North America. Canadian Institute of Mining and Metallurgy, Spec. Vol. 46, pp. 795–802.

Berzina, A.P., Berzina, A.N., Gimon, V.O., Krymskii, R.Sh., Larionov, A.N., Nikolaeva, I.V., Serov, P.A., 2013. The Shakhtama porphyry Mo ore-magmatic system (eastern Transbaikalia): age, sources, and genetic features. Russian Geology and Geophysics (Geologiya i Geofizika) 54 (6), 587–605 (764–786).

Bessonov, N.N., 2009. Revealing porphyry Mo–Cu mineralization in southeastern Transbaikalia. Vestnik Chitinskogo Gosudarstvennogo Universiteta 52 (1), 12–19.

Bierlein, F.P., McKnight, S., 2005. Possible intrusion-related gold systems in the western Lachlan Orogen, southeast Australia. Econ. Geol. 100, 385–398.

Borisenko, A.S., 1982. Heating/cooling analysis of the salt composition of solutions of gas–liquid inclusions in minerals, in: Using Fluid Inclusion Studies in Search for and Exploration of Ore Deposits [in Russian]. Nedra, Moscow, pp. 37–47.

Bowman, J.R., 1998. Stable isotope systematics of skarns, in: Lentz, D.R. (Ed.), Mineralized Intrusion-Related Skarn Systems. Mineralogical Association of Canada Short Course 26, 99–145.

Burnham, C.W., Ohmoto, H., 1980. Late-stage processes of felsic magmatism. Mining Geol., Spec. No. 8, 1–11.

Ewart, A., Taylor, S.R., 1969. Trace element geochemistry of the rhyolitic volcanic rocks, Central North Island, New Zealand. Phenocryst data. Contrib. Mineral. Petrol. 22, 127–146.

Fleck, R.J., Sutter, J.F., Elliot, D.H., 1977. Interpretation of discordant $^{40}Ar/^{39}Ar$ age spectra of Mesozoic tholeiites from Antarctica. Geochim. Cosmochim. Acta. 41, 15–32.

Garmaev, L.B., Damdinov, B.B., Mironov, A.G., 2013. Pogranichnoe Au–Bi occurrence, Eastern Sayan: Composition and link to magmatism. Geol. Ore Deposits 55 (6), 455–466.

Goldfarb, R.J., Taylor, R.D., Collins, G.S., Goryachev, N.A., Orlandini, O.F., 2014. Phanerozoic continental growth and gold metallogeny of Asia. Gondwana Res. 25 (1), 48–102.

Goryachev, N.A., Spiridonov, A.M., Vakh, A.S., Gvozdev, V.I., Budyak, A.E., 2014. The Mongol–Okhotsk orogenic belt: structural framework, endogenous events, and magmatism and metallogeny specifics, in: Correlation between the Altaides and Uralides: Magmatism, Metamorphism, Stratigraphy, Geochronology, Geodynamics, and Prediction for Metallogeny. Proceedings of the Second Rus-

sian–Kazakhstan International Meeting [in Russian]. Izd. SO RAN, Novosibirsk, pp. 35–36.

Grill, J.B., 1981. Orogenic Andesites and Plate Tectonics. Springer-Verlag, Berlin.

Hart, C.J.R., 2007. Reduced intrusion-related gold systems, in: Mineral Deposits of Canada: A Synthesis of Major Deposit Types, District Metallogeny, the Evolution of Geological Provinces, and Exploration Methods. Geological Association of Canada, Mineral Deposits Division, Spec. Publ. No. 5, pp. 95–112.

Hart, C.J.R., Baker, T., Burke, M., 2000. New exploration concepts for country-rock-hosted, intrusion-related gold systems: Tintina gold belt in Yukon, in: The Tintina Gold Belt: Concepts, Exploration and Discoveries. British Columbia and Yukon Chamber of Mines, Spec. Vol. 2, pp. 145–172.

Hart, C.J.R., Goldfarb, R.J., Lewis, L.L., Mair, J.L., 2004. The Northern Cordilleran mid-Cretaceous plutonic province: ilmenite/magnetite-series granitoids and intrusion-related mineralization. Resour. Geol. 54 (3), 253–280.

Hedenquist, J.W., Lowenstern, J.B., 1994. The role of magmas in the formation of hydrothermal ore deposits. Nature 370, 519–527.

Hoefs, J., 2015. Stable Isotope Geochemistry. Springer International Publishing, Switzerland.

Ishihara, S., 1977. The magnetite-series and ilmenite-series granitic rocks. Mining Geol. 27, 293–305.

Izbrodin, I.A., Ripp, G.S., Doroshkevich, A.G., Posokhov, V.F., 2014. Oxygen and hydrogen isotope compositions of metamorphosed high-aluminous rocks of Southwestern Transbaikalia. Dokl. Earth Sci. 459 (1), 1460–1463.

Kormilitsyn, V.S., Ivanova, A.A., 1968. Polymetallic Deposits of the Shirokinskoe Ore Field and Some Issues of Metallogeny of Eastern Transbaikalia [in Russian]. Nedra, Moscow.

Koval', P.V., 1998. Regional Geochemical Analysis of Granitoids [in Russian]. Izd. SO RAN, NITs OIGGM SO RAN, Novosibirsk.

Kovalenker, V.A., Kiseleva, G.D., Krylova, T.L., Andreeva, O.V., 2011. Mineralogy and ore formation conditions of the Bugdaya Au-bearing W–Mo porphyry deposit, eastern Transbaikal region, Russia. Geol. Ore Deposits 53 (2), 93–125.

Kozlov, V.D., 2011. Trace-element composition and origin of granitoids from the Shakhtama complex and Kukul'bei rare-metal complex (Aga zone, Transbaikalia). Russian Geology and Geophysics (Geologiya i Geofizika) 52 (5), 526–536 (676–689).

Lang, J.R., Baker, T., Hart, C.J.R., Mortensen, J.K., 2000. An exploration model for intrusion-related gold systems. Soc. Econ. Geol., Newsletter 40, 1–15.

Mair, J.L., 2004. Tectonic setting, magmatism and magmatic-hydrothermal systems at Scheelite Dome, Tombstone Gold Belt, Yukon: Critical constraints on intrusion-related gold-systems. Unpublished PhD thesis, The University of Western Australia, Perth.

Maloof, T.L., Baker, T., Thompson, J.F.H., 2001. The Dublin Gulch intrusion-hosted gold deposit, Tombstone plutonic suite, Yukon Territory, Canada. Mineral. Deposita 36, 583–593.

Marsh, E.E., Goldfarb, R.J., Hart, C.J.R., Johnson, C.A., 2003. Geology and geochemistry of the Clear Creek intrusion-related gold occurrences, Tintina Gold Province, Yukon, Canada. Can. J. Earth Sci. 40, 681–699.

McCoy, D., Newberry, R.J., Layer, P., DiMarchi, J.J., Bakke, A., Masterman, J.S., Minehane, D.L., 1997. Plutonic-related gold deposits of interior Alaska. Econ. Geol., Monograph 9, 191–241.

Meinert, L.D., Dipple, G.N., Nicolescu, S., 2005. World skarn deposit. Econ. Geol., 100th anniversary volume, 299–33.

Mel'nikov, A.V., Sorokin, A.A., Ponomarchuk, V.A., Travin, A.V., Sorokin, A.P., 2009. The Berezitovoe gold–polymetallic deposit (East Siberia): mineralogy, age, and relation with magmatism. Russian Geology and Geophysics (Geologiya i Geofizika) 50 (3), 188–194 (258–265).

Nie, F.J., Jiang, S.H., Liu, Y., 2004. Intrusion-related gold deposits of North China craton, People's Republic of China. Resour. Geol. 54 (3), 299–324.

Nikolaev, Yu.N., Prokof'ev, V.Yu., Baksheev, I.A., Chitalin, A.F., Marushchenko, L.I., Kal'ko, I.A., 2014. The first data on the zoned distribution of fluid inclusions in the ore-forming system of the Peschanka gold–copper porphyry deposit (Northeast Russia). Dokl. Earth Sci. 459 (6), 1615–1618.

Nikolaeva, L.A., Yablokova, S.V., 2007. Typomorphic features of native gold and their use during geological prospecting. Rudy i Metally, No. 6, 41–57.

Pavlova, G.G., Borisenko, A.S., Kruk, N.N., Rudnev, S.N., 2010. The age of Ag–Sb mineralization of the southeastern Pamirs and its relationship with magmatism. Izvestiya Sibirskogo Otdeleniya RAN Sektsiya Nauk o Zemle. Geologiya, Poiski i Razvedka Rudnykh Mestorozhdenii 36 (1), 60–67.

Pavlova, N.V., Tikhomirov, I.N., 1964. The Shakhtama complex, in: Intrusive Complexes of Transbaikalia [in Russian]. Nedra, Moscow, pp. 155–164.

Peccerillo, A., Taylor, S.R., 1976. Geochemistry of Eocene calc-alkaline volcanic rocks from the Kastamonu area, Northern Turkey. Contrib. Mineral. Petrol. 58 (1), 63–81.

Petrovskaya, N.V., 1973. Native Gold [in Russian]. Nauka, Moscow.

Prokof'ev, V.Yu., Bortnikov, N.S., Zorina, L.D., Kulikova, Z.I., Matel', L.N., Kolpakova, N.N., Il'ina, G.F., 2000. Genetic features of the Darasun gold–sulfide deposit (eastern Transbaikal region). Geol. Ore Deposits 42 (6), 474–495.

Pirajno, F., 2009. Hydrothermal Processes and Mineral Systems. Springer, Berlin.

Prokof'ev, V.Yu., Volkov, A.V., Sidorov, A.A., Savva, N.E., Kolova, E.E., Uyutnov, K.V., Byankin, M.A., 2012. Geochemical peculiarities of ore-forming fluid of the Kupol Au–Ag epithermal deposit (Northeastern Russia). Dokl. Earth Sci. 447 (2), 1310–1313.

Ramdohr, P., 1960. Die Erzmineralien und Ihre Verwachsungen. Akademie-Verlag, Berlin.

Redin, Yu.O., Kozlova, V.M., 2014. Gold–bismuth–telluride mineralization in ores from the Serebryanoe deposit of the Lugokan ore cluster of eastern Transbaikalia. Russ. J. Pacific Geol. 8 (3), 187–199.

Redin, Yu.O., Kalinin, Yu.A., Nevol'ko, P.A., Kirillov, M.V., Kolpakov, V.V., 2014. Mineral assemblages and zoning of mineralization of the Lugokan ore cluster (eastern Transbaikalia). Geologiya i Mineral'no-Syr'evye Resursy Sibiri 18 (2), 83–93.

Redin, Yu.O., Dultsev, V.F., Nevolko, P.A., 2015. Gold–bismuth mineralization of the Lugokan ore field (Eastern Transbaikalia): Age, mineral composition and relationship with magmatism. Ore Geol. Rev. 70, 228–240.

Rickwood, P.C., 1989. Boundary lines within petrologic diagrams which use oxides of major and minor elements. Lithos 22 (4), 247–263.

Roedder, E., 1984. Fluid Inclusions. Mineralogical Society of America, Washington, D.C.

Rombach, C.S., Newberry, R.J., 2001. Genesis and mineralization of the Shotgun deposit, southwestern Alaska. Mineral. Deposita 36, 607–621.

Rowins, S.M., 2000. Reduced porphyry copper–gold deposits: A new variation on an old theme. Geology 28, 491–494.

Savva, N.E., Preis, V.K., 1990. Atlas of Native Gold of the Northeastern USSR [in Russian]. Nauka, Moscow.

Sazonov, V.D., 1978. Porphyry copper mineralization in Transbaikalia. Geologiya Rudnykh Mestorozhdenii 20 (2), 95–98.

Seal II, R.R., 2006. Sulfur isotope geochemistry of sulfide minerals. Rev. Mineral. Geochem. 61 (1), 633–677.

Sidorenko, V.V., 1961. Geology and Petrology of the Shakhtama Intrusive Complex [in Russian]. Izd. AN SSSR, Moscow.

Sillitoe, R.H., 1991. Intrusion-related gold deposits, in: Gold Metallogeny and Exploration. Blackie & Son Ltd., Glasgow, pp. 165–209.

Sizykh, Vit.I., Sizykh, Val.I., 2001. The ore potential of postcollisional structures in Transbaikalia, in: Postcollisional Evolution of Mobile Belts. Abstracts of an International Scientific Conference [in Russian]. Izd. UrO RAN, Yekaterinburg, pp. 175–178.

Skurskii, M.D., 1996. The Interior of Transbaikalia [in Russian]. GCh-TU, Chita.

Sotnikov, V.I., Berzina, A.P., Nikitina, E.I., Proskuryakov, A.A., Skuridin, V.A., 1977. Copper–Molybdenum Ore Association (by the Example of Siberia and Adjacent Regions) [in Russian]. Nauka, Novosibirsk.

Spiridonov, A.M., Zorina, L.D., Kitaev, N.A., 2006. Gold-Bearing Ore-Magmatic Systems of Transbaikalia [in Russian]. Akadem. Izd. GEO, Novosibirsk.

Spiridonov, E.M., 2010. A review of gold mineralogy in major types of Au mineralization, in: Gold of the Kola Peninsula and Adjacent Regions. Proceedings of the All-Russian (with non-Russian Participants) Scientific Conference Dedicated to the 80th Anniversary of the Kola Research Center of the Russian Academy of Sciences [in Russian]. Izd. K & M, Apatity, pp. 143–171.

Tauson, L.V., 1982. Geochemistry and metallogeny of latite series. Geologiya Rudnykh Mestorozhdenii, No. 3, 3–14.

Tauson, L.V., Gundobin, G.M., Zorina, L.D., 1987. Geochemical Fields of Ore-Magmatic Systems [in Russian]. Nauka, Novosibirsk.

Timofeevskii, D.A., 1972. Geology and Mineralogy of the Darasun Gold Ore District [in Russian]. Nedra, Moscow.

Thompson, J.F.H., Sillitoe, R.H., Baker, T., Lang, J.R., Mortensen, J.K., 1999. Intrusion-related gold deposits associated with tungsten–tin provinces. Mineral. Deposita 34, 323–334.

Travin, A.V., Yudin, D.S., Vladimirov, A.G., Khromykh, S.V., Volkova, N.I., Mekhonoshin, A.S., Kolotilina, T.B., 2009. Thermochronology of the Chernorud granulite zone, Ol'khon region, western Baikal area. Geochem. Int. 47 (11), 1107–1124.

Zorin, Yu.A., Zorina, L.D., Spiridonov, A.M., Rutshtein, I.G., 2001. Geodynamic setting of gold deposits in Eastern and Central Trans-Baikal (Chita Region, Russia). Ore Geol. Rev. 17, 215–232.

Zorina, L.D., 1993. Genetic model of gold deposits in the tectonic-magmatic structures of the central type. Geologiya i Geofizika (Russian Geology and Geophysics) 34 (2), 77–83 (73–78).

Editorial responsibility: A.S. Borisenko